

**COLLOIDAL FILTRATION OF ALUMINA-ZIRCONIA
WITH SOLID OXIDE ADDITIVES**

HAKIMEH WAKILY

DISSERTATION SUBMITTED IN FULFILLMENT OF THE
REQUIREMENTS FOR THE DEGREE OF
MASTER OF ENGINEERING SIENCE

FACULTY OF ENGINEERING
UNIVERSITY OF MALAYA
KUALA LUMPUR-MALAYSIA

AUGUST 2012

UNIVERSITY MALAYA
ORIGINAL LITERARY WORK DECLARATION

Name of Candidate: Hakimeh Wakily

I.C/Passport No:

Registration/Matric No: KGA080044

Name of Degree: Master of Engineering Science

Title of Project Paper/ Research Report/ Dissertation/ Thesis (“This Work”):

Colloidal Filtration of Alumina-Zirconia with Solid Oxide Additives

Field of Study: Ceramic Composite

I do solemnly and sincerely declare that:

- (1) I am the sole author/writer of this Work;
- (2) This work is original;
- (3) Any use of any work in which copyright exists was done by way of fair dealing and for permitted purpose and any excerpt from, or reference to or reproduction of any copyright work has been disclose expressly and sufficiently and the title of the Work and its authorship have been acknowledge in this Work;
- (4) I do not have any actual knowledge nor do I ought reasonably to know that the making of this work constitutes an infringement of any copyright work;
- (5) I hereby assign all and every rights in the copyright to this work to the University of Malaya (UM), who henceforth shall be owner of the copyright in this work and that any written consent of UM having been first had and obtained;
- (6) I am fully aware that if in the course of making this work I have infringed any copyright whether intentionally or otherwise, I am be subject to legal action or any other action as may be determined by UM.

Candidate’s Signature Date

Subscribed and solemnly declared before,

Witness’s Signature Date

Name:

Designation:

ABSTRAK

Komposit seramik homogeny Alumina dan Zirkonia (3 mol % yttria distabilkan oleh Zirkonia) dengan amaun kecil pepejal oksida disediakan menggunakan metod penapisan koloid. Objektif penggunaan Zirkonia adalah untuk menghasilkan Zirkonia yang diperkuatkan dengan alumina (ZTA) bersama 15wt% Zirkonia. Bagi meningkatkan mikrostruktur serta kemampatan ZTA, lebih kurang 0.5wt% magnesia ditambah. Lubrikan pepejal Oksida (CuO) ditambah dengan kuantiti yang kecil (≤ 1 wt %) bagi menghasilkan pelinciran tindakan sendiri bagi mengurangkan pekali geseran kering. Suspensi Alumina beserta material fasa ke dua disediakan menggunakan pelbagai tambahan pepejal dan kepekatan surfaktan. Dolapix CE64 dan Tiron digunakan sebagai surfaktan dan kesan ke atas kestabilan suspense particle pepejal oksida disiasat. Sifat suspensi reologi dipelajari dengan mengukur potensi zeta dan suspensi viskosi. Kesudahan campuran dijadikan palet sampel menggunakan penapisan koloid. Proses disudahkan dengan pensinteran kurang tekanan dengan 1550 °C. Fasa, saiz bijiran dan analisis komposisi kualitatif dijalankan menggunakan pembelauan X-ray (XRD) dan pengimbasan imej mikroskopi elektron (SEM). Ketumpatan sebatian hijau dan sinter diukur menggunakan metod Archimedes dan sifat mekanikal dinilai dengan kekerasan dan kekuatan keliatan pengukuran. Sifat komposit Trobologi disiasat menggunakan ujian kehausan dan pekali geseran yang berlaku bagi kompaun yang berlainan terhadap bola Zirkonia. Ujian ketumpatan menunjukkan ketumpatan penuh (>99%) dicapai bagi. Komposit ZTA bersama MgO menunjukkan nilai kekerasan yang tinggi (sehingga 20 GPs) dan peningkatan kekuatan keliatan ($3.7 \text{ MPa.m}^{-1/2}$). Mgo-CuO yang ditambahkan ZTA juga menunjukkan nilai kekerasan dan kekuatan keliatan yang tinggi; setinggi 19.7 GPs dan $4 \text{ MPa.m}^{-1/2}$ masing-masing. Ketahanan

kehausan CuO yang ditambahkan ZTA bertambah baik manakala sedikit kekurangan pada pekali geseran dengan jarak bagi CuO yang ditambah komposit Zirkonia.

ABSTRACT

Homogeneous ceramic composites of alumina and zirconia (3 mol % yttria stabilized zirconia) with small amount of solid oxides were prepared using colloidal filtration method. The purpose of using zirconia was to provide zirconia toughened alumina (ZTA) including 15wt% zirconia. And to improve the microstructure and density of ZTA, less than 0.5 wt% of magnesia was added. Solid oxide lubricant (CuO) was doped in small quantities (≤ 1 wt %) to provide a self-lubrication action and thereby to decrease the coefficient of dry friction. Suspension of alumina as well as the second phase materials was prepared with various solid loadings and various concentrations of surfactant. Dolapix CE64 and Tiron were used as surfactant and their influence on the stability of solid oxide particles in suspension was investigated. The rheological properties of suspension were studied by measuring zeta-potential and viscosity. The satisfactory mixtures were made into sample pallets using colloidal filtration. The process was completed with pressurless sintering in 1550 °C. Phase, grain size and qualitative compositional analysis were done using X-ray diffraction (XRD) and scanning electron microscopy (SEM) images. Density of green and sintered compounds was measured using Archimedes method. The mechanical properties evaluated by hardness and fracture toughness measurements (Vickers indentation method). The tribological properties of composites were investigated by wearing test and coefficient of friction procured for different compound against the zirconia ball. Densification studies show that near full density ($>99\%$) was obtained. ZTA composite with MgO shows high value of hardness (up to 20 GPs) and enhanced fracture toughness ($3.7 \text{ MPa}\cdot\text{m}^{-1/2}$). MgO-CuO doped ZTA also presents high value for hardness and fracture toughness (19.7 GPs and $4 \text{ MPa}\cdot\text{m}^{-1/2}$ respectively). Wearing resistant of CuO-doped ZTA was improved and coefficient of friction for CuO-doped composite against zirconia shows slightly decreases with distance.

ACKNOWLEDGMENT

I am deeply thankful to my supervisor, Dr. Ibrahim Henk Metselaar for his help and guidance throughout this research.

The writing of this research has been a worthwhile experience and I have learned a lot from it. I believe that I was not able to complete this work without the support of many people; here I would like to thank to all of them.

I also like to express my appreciation to the University of Malaya for providing laboratory facilities and supporting this project financially.

I owe heartfelt and much deserved thank-you to my beloved family for their love and encouragement and I dedicate this work to them.

TABLE OF CONTENT

ABSTRAK	i
ABSTRACT	iii
ACKNOWLEDGMENT	iv
TABLE OF CONTENT	v
LIST OF FIGURES	viii
LIST OF TABLES.....	x
LIST OF ABBREVIATIONS	xi
LIST OF SYMBOLS	xii
CHAPTER 1 INTRODUCTION	1
1.1 Background.....	1
1.2 Importance of study	2
1.3 Research problem statement	3
1.4 Objectives	4
1.5 Outline of study	4
CHAPTER 2 LITERATURE REVIEW	7
2.1 . Ceramic Materials and Ceramic Composites	7
2.2 Aluminum Oxide	7
2.2.1 Influence of Magnesia on Alumina.....	9
2.3 Zirconium Dioxide	10
2.3.1 Fully Stabilized Zirconia.....	12
2.3.2 Partially Stabilized Zirconia (PSZ)	12
2.4 Toughening Methods in Ceramics.....	12
2.4.1 Zirconia Toughened Alumina (ZTA) Composite	13
2.5 Ceramic Processing	14
2.6 Colloidal Filtration Method	17
2.6.1 Particle Segregation during Filtration	17
2.6.2 Cast Formation Time	19
2.7 Colloidal suspension.....	19
2.8 The Stability of Colloidal Dispersions	22

2.9 Stabilizing Method in Ceramic Suspensions	22
2.9.1 Dolapix CE 64.....	24
2.9.2 Tiron.....	25
2.10 Density and Porosity Measurements	26
2.11 Firing	27
2.12 Mechanical Properties	28
2.12.1 Hardness.....	29
2.12.2 Fracture Toughness.....	29
2.13 Wear and friction.....	31
2.14 Wear in ceramics	32
2.15 Solid-state lubrication.....	34
CHAPTER 3 RESEARCH EXPERIMENTAL DESIGN	35
3.1 Introduction.....	35
3.2 Material.....	37
3.3 Preparation of Single phase suspension.....	38
3.4 Zeta Potential, pH and Viscosity	39
3.5 Preparation of suspension of different Oxides	41
3.6 Filtration Procedure	43
3.7 Characterization of Green samples	44
3.8 Sintering.....	44
3.9 Sample Preparation.....	44
3.10 Sample Characterization.....	46
3.10.1 Vickers Hardness (HV) and fracture toughness.....	46
3.10.2 X-Ray Analysis	46
3.10.3 Scanning Electron Microscope (SEM)	47
3.11 Wearing test.....	48
CHAPTER 4 RESULTS AND DISCUSSION	50
4.1 Suspension analyses	50
4.1.1 Zeta potential	50
4.1.2 Viscosity	54
4.1.3 pH.....	55
4.2 Sample Characterisation	57

4.2.1 Density	57
4.2.2 Microstructure and XRD.....	58
4.3 Mechanical properties.....	67
4.3.1 Hardness and fracture toughness	67
4.3.2 Wearing.....	72
CHAPTER 5 CONCLUSION AND RECOMMENDATION	75
5.1 Conclusion.....	75
5.2 Recommendation	76
REFERENCES	78
APPENDIX A: ZETA POTENTIAL MEASURIMENT.....	81
APPENDIX B: X-RAY DIFFRACTION	88
APPENDIX C: SEM IMAGE OF VICKERS INDENTATION	91

LIST OF FIGURES

Figure 1.1 flowchart of this project.....	6
Figure 2.1 Phase diagram of YSZ.....	11
Figure 2.2 Illustration of transformation toughening in an alumina matrix containing ZrO ₂ particles.	14
Figure 2.3 Chemical structure of the dispersant.....	25
Figure 2.4 Tiron (a) structural formula and (b) 3D view	26
Figure 2.5 Cracks at an indent allow determination of K_{IC}	31
Figure 3.1 production procedure	36
Figure 3.2 SV-10 series vibro viscometers.	41
Figure 3.3 A and B: general part of a filtration equipment; C: The glass filter used in this work.....	43
Figure 3.4. a: Pin-on-disc wearing machine; b: specimen fixed with epoxy inside suitable sample holder, and zirconia ball inside holder	49
Figure 4.1 Zeta-potential of Al ₂ O ₃ , 3Y-TZP, CuO and MgO as a function of pH without any surfactant.	51
Figure 4.2. Zeta-potential of alumina, yttria stabilised zirconia, magnesia and copper (II) oxide in the a: presence of 0.4 wt % DolapixCE64 and b: presence of 0.5 wt% Tiron as a function of pH.	53
Figure 4.3 The pH change with increasing solid concentration in the presence of 0.4 wt% Dolapix and 0.5 wt% of Tiron (a): in alumina and yttria stabilised zirconia suspension; (b): in magnesia and copper (II) oxide suspension.	56
Figure 4.4 SEM image of polished and thermally etched	59
Figure 4.5. XRD of thas-received 3Y-TZP powder.	60
Figure 4.6 The SEM image of the polished and thermally etched 3Y-TZP. The ceramic sintered at 1550 °C for 2 h in air.	60
Figure 4.7 X- Ray diffraction pattern of sintered samples of Alumina, 3Y-TZP and ZTA.....	61
Figure 4.8 SEM micrograph of homogeneous ZTA (85wt% alumina and 15wt% 3Y-TZP), the bright area represents 3Y-TZP and dark area represents alumina particles.	63
Figure 4.9. SEM image of ZTA, white color represents zirconia grain and gray color represents alumina particles.	63

Figure 4.10 SEM of ZTA composite with 0.5wt% MgO, sintered, polished and thermally etched, the arrows point MgO particles	64
Figure 4.11 SEM micrograph taken from three different point at cross section of ZTA+ 0.5 wt% MgO samples prepared from A: suspension dispersed by Tiron; B: suspension dispersed by Dolapix	65
Figure 4.12 SEM of ZTA with 1 wt% CuO, the composite.....	66
Figure 4.13 SEM image of ZTA with 0.05 wt% MgO and 0.1 wt% CuO; the gray area presents alumina, bright area presents zirconia and very small white spot pointed by arrows are the CuO and MgO particles.....	67
Figure 4.14 Vickers hardness value for different composites in 10 Kg load on the polished surface before and after thermal etching	69
Figure 4.15 Fracture toughness (K_{IC}) value for different compound calculated with Antis-Casellas factors and general formula	71
Figure 4.16 Coefficient of friction changes with sliding distance (m) up to 3600m for sintered, polished and thermally etched samples.	73
Figure 4.17 The worn volume (mm^3) for different compounds as a function of the sliding distance at a sliding speed of 0.1 m/s with zirconia ball.	74

LIST OF TABLES

Table 2.1 Some of basic forming methods.....	15
Table 3.1 Properties of starting material.	37
Table 3.2 Properties of two different dispersants.....	38
Table 3.3 Characteristic of initial single phase suspension.....	39
Table 3.4 Characteristic of mixed suspension of different Oxides	42
Table 4.1 Apparent viscosity η_a for different suspensions.	55
Table 4.2 The average density, shrinkage and porosity obtained for different compounds prepared using the suspensions with cod numbers taken from table 3.3 and 3.4.....	57

LIST OF ABBREVIATIONS

3Y-TAP	Yttria Stabilised Zirconia
Dolapix	Dolapix CE64
HV	Vickers Hardness
LOM	Light Optical Microscope
PSZ	Partially Stabilised Zirconia
PZC	Point of Zero Charge
TZP	Tetragonal Zirconia Polycrystal
SEM	Scanning electron Microscope
XRD	X-Ray Diffraction
ZTA	Zirconia Toughened Alumina
ZTAc	Zirconia toughened Alumina Composite

LIST OF SYMBOLS

A	Area
c	Cracks length
°C	Degree Celsius
Cm ³	Cubic Centimeter
E	Elasticity Modulus
E(R)	Repulsion energy
E (A)	Attraction energy
E'	Elasticity Modulus-Initial
F	Force
f	Coefficient of friction
$f (K_a)$	Henry's function
g	Gram
GPa	GigaPascal
ΔG	Gibbs free energy
K_{IC}	Fracture toughness
Kg	Kilogram
k_w	Specific wear rate
L_c	Cast permeability
L	Length
η	Viscosity
Pa.s	Pascal-second
MPa	Mega Pascal
M	Meter
mm	Millimeter

mm/S	Millimeter per Second
N	Newton
P	Load
Pa	Pascal
ρ	Density
ρ_s	Density of suspension
$\rho_{p,i}$	Density of particles type i
$r_{p,i}$	Particle radius type i
δ_c	cast thickness
T	Temperature
T_m	Temperature- Melting
Φ_c	Cast concentration
Φ_s	Suspension concentration
ε	Porosity of the cast
ε	Dielectric constant
δ_{dense}	Cast thickness
ΔP	Pressure difference
R_f	Filter resistant
r_p	Particle radius
U_E	Electrophoretic mobility
v_c	sedimentation velocity
V_w	Wear Volume
Vol	Volume
W	Weight

CHAPTER 1 INTRODUCTION

1.1 Background

An essential challenge in the preparing and developing of engineering compounds is to combine incompatible properties such as hardness, toughness and wear resistant to achieve a high performance in the same component. A possible concept to approach this demand is to design composite material. The main quality in a composite is to obtain the homogenous structure of matrix and reinforcement material which inheritances the mechanical properties from both matrix and continually dispersed elements. A wide variety of advanced methods are applied for production of ceramic composite materials which they have been developed from basic available routes, such as powder processing, plastic forming or consolidation of the ceramic slip. In between colloidal filtration is a suitable technique for fabrication of a uniform ceramic composite because it is using a homogeneous dispersed mixture of different powder dispersed in a stable suspension. Colloidal filtration technique consists of two steps: preparation of a stable suspension of different ceramic powders and separation of mixed particles from liquid in a form of compact substance by filtration. An external force such as pressure or vacuum is employed when obtaining a dense compound is essential to achieve. The dried substance is a close packed powder compact that needs to sinter to achieve fully dense material components with high value of mechanical properties.

Moreover, the method used in this study is a low cost, rapid, near net shaping process, easy to implement and capable of producing dense homogeneous composite of ceramics with different range of initial particle size.

1.2 Importance of study

Dispersing tough particles in a ceramic matrix is a frequent reinforcing method in composite field. However in most used ceramic processing techniques, same as powder pressing, it is difficult to achieve a homogeneous scattering of second phase. And it will be more difficult when the particle are in micro and nanometer range. Propitiously with colloidal processing rout there is a great success in producing uniform structure composite. This work presents the study on colloidal filtration technique and preparation of stable suspension with unique dispersion of particles.

Furthermore in this work magnesia and copper (II) oxide are used as sintering aid and preparing solid lubrication system in ceramic composite. While in the literature there are some reports of application of sintering aid material and solid phase lubricant oxides in ceramic compound and in most of case the applied processing is powder pressing. Conversely when the colloidal processing is used there is no report of using doped material. For instance magnesia has a great beneficial influence on the sintering process of alumina based ceramics but there is a few works about the stability properties of aqueous suspension of magnesia or its affect on the colloidal solution of alumina.

This study presents an experiments for wearing resistant measurements of Al_2O_3 , 3Y-TZP and their composites with doped amount of CuO and MgO, which were tested against the zirconia (ball) and the coefficient of friction as well as wear volume were measured, however in the most of previous works the wearing resistant of ceramics have been not studied against of zirconia, and the reported value for coefficient of friction for ceramic compounds is against alumina.

1.3 Research problem statement

Zirconia toughened alumina (ZTA) is a well known ceramic composite (Wang and Stevens, 1989) ; (Nevarez-Rascon et al., 2009) and has a lot of application in industry and recently in biology as implants in different part of body (Chevalier, 2006) . During the years a lot of methods have been developed for fabrication of dense ZTA which in all of them the aim is to achieve homogeneous composite of alumina and zirconia.

To date the most common method to fabricate ZTA composite is powder metallurgy, but the level of homogeneity achieved by this method is not satisfying, particularly when small amount of other oxides as a sintering aid or lubricant are necessary to use the homogeneity is more demolished. The homogeneity could be improved by applying colloidal preparation method but it is effective for ZTA composite with low fraction of zirconia (Rafferty et al., 2009). More over in these methods the particle morphology is of extreme importance. Irregularly shaped particles cause a lot of internal friction during compacting and they may result in high internal stresses or crack formation. Besides that the irregular shape may also be a cause of bad stacking of the powder during filling of the mould. The presence of defects and inhomogeneities has a large negative effect on the properties of the ceramics such as hardness, toughness and strength.

On the other hand in most of powder compacting methods to obtain high density the hot isostatic press is required which is high cost procedure.

Colloidal processing of ceramics is a preferred route to obtain near net shape components with a homogeneous and defect free structure (Maarten Biesheuvel and Verweij, 2000);(Micháľková et al., 2010) . For suspension processing the particle shape is of less importance, since in these processes the powder particles are de-agglomerated before the

consolidation step. Here by applying a simple colloidal filtration method, dense compacts of ZTA was prepared which the microstructure studies approved that the zirconia particles are dispersing consistently among the alumina matrix. Choosing magnesium oxide (MgO) additive which is suggesting as a sintering aid for alumina ceramic and ZTA composite by many other researchers, (Szutkowska, 2004), (Dey and Biswas, 2009) and (Azhar et al., 2011) helps to improve the sintered density and mechanical properties of both CuO - doped and un-doped ZTA composites.

1.4 Objectives

The objectives of this research were:

- 1) To prepare homogeneous ceramic composites of alumina and zirconia(zirconia toughened alumina) using colloidal filtration method
- 2) To Study the stability and rheological properties of the ceramic suspension in the presence of two different dispersions (Dolapix CE64 and Tiron) by measuring the zeta potential and viscosity in different concentration.
- 3) Improving the microstructure, density, hardness and fracture toughness of ZTA composite by doping with small amount of magnesia.
- 4) Studying the tribological properties, coefficient of friction and wearing resistant in the non-doped, CuO-doped and CuO-MgO- doped ZTA composites.

1.5 Outline of study

The research outlines are as follows:

- Literature review

The theories and concept of ceramic composites material, toughening methods of zirconia toughened alumina and colloidal route were reviewed from various sources such as text books, journals, previous dissertation reports and world wide websites. Review of literatures is presented in chapter 2.

- Experimental works and characterization

This part includes preparation of suspension of Al_2O_3 and 3Y-TZP and doped oxides with different surfactants, filtration and sintering. After preparation process, phase identification of composites is analyzed by X-ray diffraction and scanning electron microscope (SEM) is used to observe the microstructure of the compounds. The hardness, fracture toughness and wearing resistance of composite is measured. The characterization techniques are also described in chapter 3.

- Results and discussion

The result of experiments and comparative study on the results is collected in chapter 4. Discussion about obtained results in this work and the reliability of data also is presented in chapter 4.

- Conclusion and recommendation

Conclusion of present study and useful recommendation for future research are presented in chapter 5.

The methodology of this research is shown in the following flowchart.

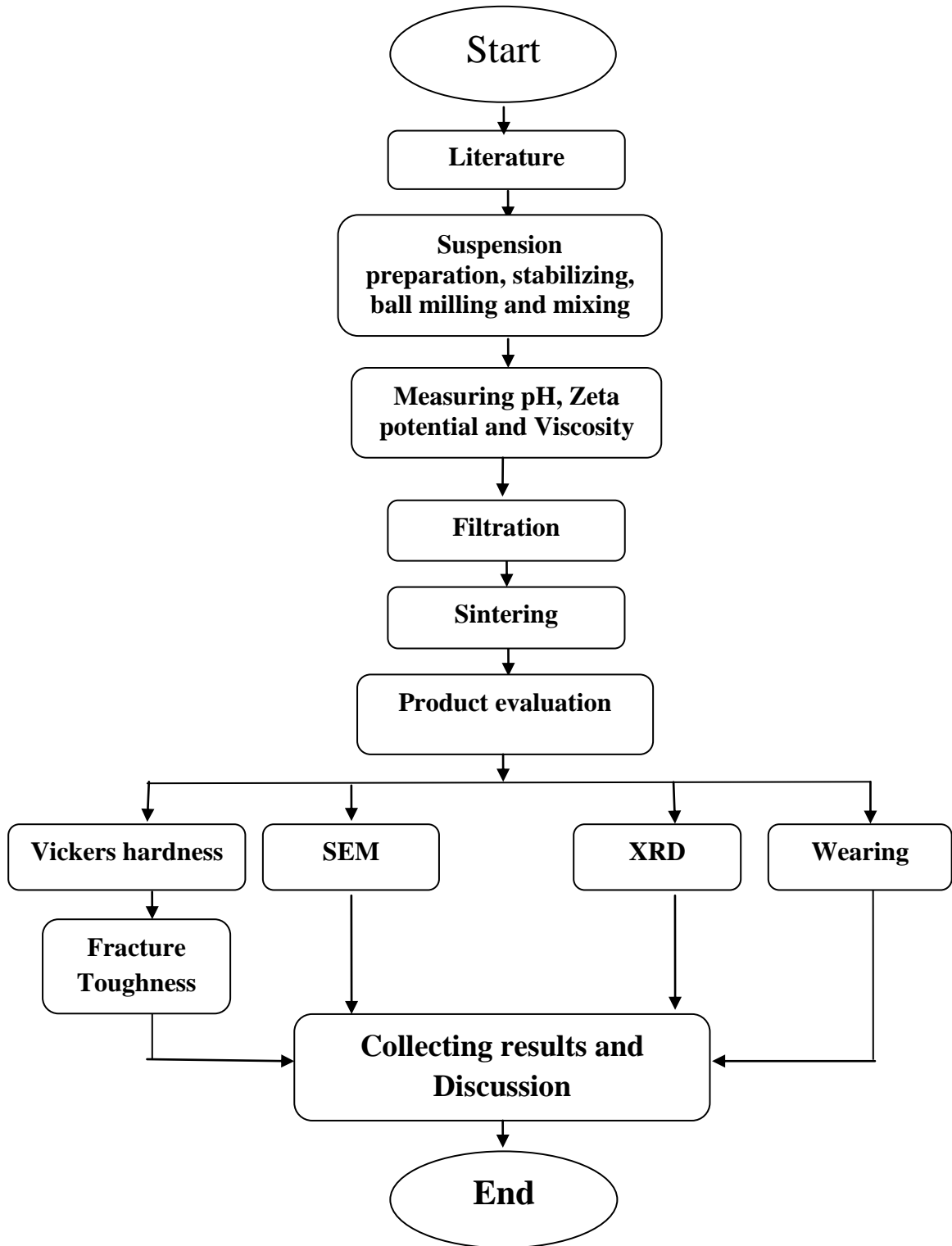


Figure 1.1 flowchart of this project

CHAPTER 2 LITERATURE REVIEW

2.1 . Ceramic Materials and Ceramic Composites

Ceramic materials are defined as materials that are neither organic nor metal; they are generally connected with mixed bonding, combination of covalent, ionic and sometimes metallic. They consist of an array of interconnected atoms, there are no distinct molecules. Most commonly they are oxides, carbides and nitrides. Excellent properties are presented, especially high hardness and high melting temperature, chemical inertia and low heat conductivity and electricity. However, it has an unwanted property normally brittleness. The brittleness is a tendency to initiate and spread of cracks and it is very important when we want to assess and characterize the ceramic materials. The functions of ceramic products depend on their chemical composition and microstructure, which determines their properties. Composites are the combinations of more than one material or phase including matrix and reinforcement which one or both can be made from ceramic materials (Carter and Norton, 2007).

Nowadays, the applications of advanced ceramics and their composites are developed in biomedical, cutting tools, semiconductors technology, coating and others.

2.2 Aluminum Oxide

Aluminum oxide, Al_2O_3 or alumina, appears in several crystalline forms, of which alpha or corundum is the most stable and most dense. Corundum has a trigonal bravais lattice where the crystallographic structure consists of oxygen atoms in HCP (Hexagonal Close-Packing) where the alumina atoms occupy 2/3 of the octahedral holes. These are connected to each other. The theoretical density is 3.97 g/cm^3 (Riedel, 2000). The principal

sources of purified alumina and hydrated alumina are native bauxites and laterites, from which alumina is extracted by the Bayer process, in which the mineral is pulverized, melted with soda, separated, and calcined. Four types of alumina are usually used in ceramic products: calcined, tabular, fused, and hydrated. Alpha alumina melts at 2040°C, with creeping and sintering beginning at 1750°C. Mineralizers and fluxers permit sintering at lower temperatures (Harper, 2001). It is superior to most other oxide ceramics in mechanical, thermal, and electrical properties but as all ceramics have low resistance to cracking. The raw materials are plentiful, low in cost, and amenable to fabrication by a wide variety of techniques into the selected shapes. They find to use in spark plugs, pumps, refractory lining, missile nose cones, electrical power insulators, abrasives and cutting tools, and in many ways in electronics packaging. A possible way to achieve better quality is to use fine powder of Al_2O_3 and apply high pressure sintering to avoid grain growth. With HIP (Hot Isostatic Pressing) pieces without porosity can be obtained. Furthermore, a small amount of MgO can be added to avoid grain growth. Without this additive, the grains can grow until a size of 50 μm . large grains usually imply that there is a bigger quantity of porosity.

Numerous researchers have reported that the addition of a second phase, a process referred to as toughening, can increase the strength and toughness of alumina. Schwartz discusses the properties of alumina toughened by additions of various forms of zirconia, and by additions of silicon carbide (SiC) or titanium carbide (TiC) (Schwartz, 1991).

Alumina-based ceramics in general show better wear resistance than zirconia due to their higher hardness. Furthermore the larger thermal conductivity of alumina-based ceramics contributes to enhanced tribological properties. The abrasive wear resistance of alumina is very good, but alumina is very susceptible to wear transitions due to increasing load and

sliding velocity, which transitions from mild to severe wear occurs is the higher load for ZTA.

2.2.1 Influence of Magnesia on Alumina

Commercially available alumina powders usually include some impurities that affect the decisive material properties. Most of these impurities are not soluble in alumina and, at the high temperatures forms a slight liquid phase in the region of the alumina particles that leads to abnormal grain growth. Hence, in alumina, some type of additive is used to develop the sintering process and/or inhibit anomalous grain growth since large grains have diminished influence on the mechanical strength.

There exist many possible additives, mainly metal oxides which, with various efficiencies, act as sintering aids and grain growth inhibitors. The most used and also the most effective one is magnesia (MgO). Because of its efficiency, very small amounts of MgO are needed for good densification and to limit abnormal grain growth during sintering of alumina. The role of magnesia in alumina was summarized in a historical review on the subject (Bennison and Harmer, 1983). However, most of the studies done so far have been focused on understanding the microstructural effect of MgO in the sintering process and There are few works, which consider other effects of MgO, for example, in slip rheology or the forming process, which also will have a considerable impact on the final microstructure of alumina. An important factor about MgO is its strongly basic nature and very high isoelectric point, which is in pH 10.5-11.5. This makes some difficulties in perfectly dispersing and stabilizing MgO particles using conventional dispersants such as polyelectrolytes. In addition, MgO has a high solubility in acidic and neutral conditions which make it impossible to use pure electrostatic stabilization at low pH, which is otherwise a common way to stabilize alumina particles (Tari et al., 1997).

2.3 Zirconium Dioxide

Zirconia (ZrO_2) has been used in the refractory industry for close to a century, but only recently has advanced and stabilized fine-grained zirconia comes into widespread use in electro ceramics and medical application such as dental restoration. The combination of hardness, good thermal insulation, chemical inertness, high density, low coefficient of friction, expansion coefficient close to that of steel, and high fracture toughness has made various forms of zirconia attractive for many applications. Zirconia is usually produced from zircon, ZrSiO_4 . The first step is to convert zircon to zirconyl chloride by melting the zircon with sodium hydroxide to form Na_2ZrO_3 . This compound is then treated with HCl to form zirconyl chloride, $\text{ZrOCl}_2 \cdot 8\text{H}_2\text{O}$. There are two ways to make zirconia from zirconyl chloride: thermal decomposition which is more economic, but the resulting material is not usually of as high purity and fine particle size as that produced by the precipitation method includes chemical reactions to obtain the zirconia hydroxides as an intermediate material. A final calcination process results in zirconia powder. By controlling condition of the precipitation and calcination, it is possible to acquire desired particle size and shape, grain size, and specific surface area (Harper, 2001, Cardarelli, 2008).

Zirconia forms in three crystalline structures: monoclinic, tetragonal, and cubic. From room temperature to 1170°C the structure is monoclinic (m), then it transforms to tetragonal (t). It remains tetragonal until about 2370°C , when it converts to cubic (c). Pure ZrO_2 sintered above 1170°C spontaneously disintegrates during cooling because of the tetragonal to monoclinic transformation that involves an increase in density from 5.7 to over 6 g/cm^3 and implies an increase of the volume of $\sim 5\%$. This transformation happens without diffusion, and it is martensitic character. The grains of tetragonal zirconia are

transformed from tetragonal to monoclinic if a tensile stress is present. The growth of a crack implies a tensile stress, which is counteracted by the volume increase. This tends to terminate the crack propagation. For applications involving temperatures over 1000°C, zirconia must be stabilized to prevent the phase inversion, which is usually destructive. Figure 1.1 shows the phase diagram of zirconia with the addition of yttria by mole. Unstabilized zirconia, with density of 6.05 g/cm³ has many uses as grinding medium, or added to alumina or magnesia it promotes sinterability and enhances strength and other properties. The stabilization may be either partial or full, depending on the amount of stabilizer added(Harper, 2001).

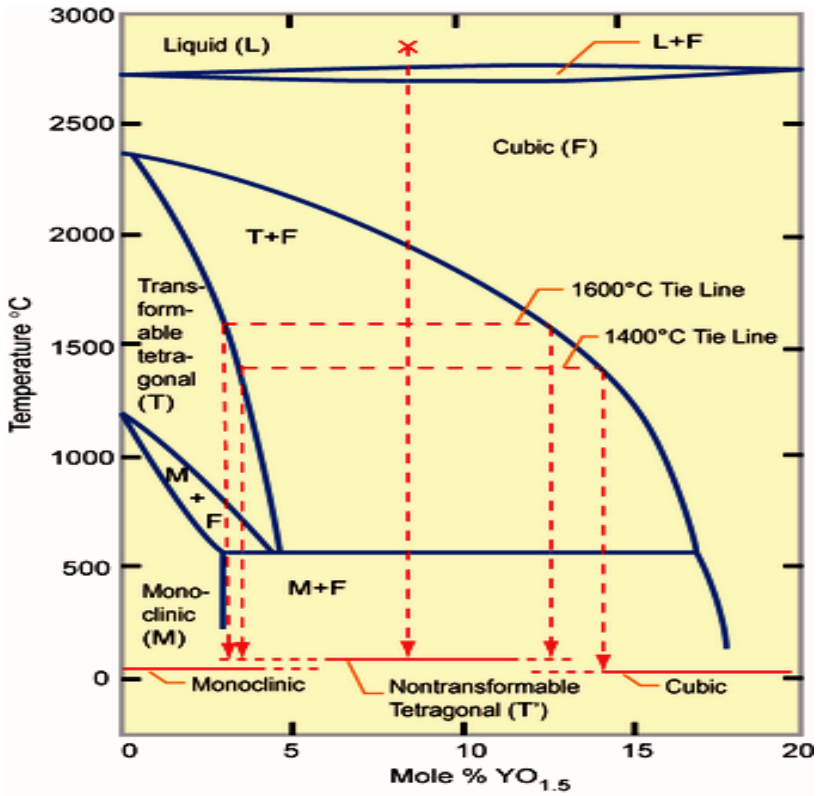


Figure 2.1 Phase diagram of YSZ

2.3.1 Fully Stabilized Zirconia

To prevent the destructive monoclinic-to-tetragonal phase inversion during firing and cooling, stabilizers such as CaO, MgO, Ce₂O₃ and Y₂O₃ is used. The composition, called stabilized zirconia, retains the cubic structure without the critical inversion during cooling. For zirconia to be fully stabilized, more than 16 mol% CaO, 16 mol% MgO, or 8 mol% Y₂O₃ must be added (Harper, 2001).

2.3.2 Partially Stabilized Zirconia (PSZ)

Partially stabilized zirconia contains an insufficient amount of calcia, magnesia, or yttria stabilizing compound to obtain a cubic plus metastable tetragonal ZrO₂. Partially stabilized zirconia has been found to have higher strength and toughness. The partially stabilized zirconia is also known as tetragonal zirconia polycrystal (TZP). Transformation toughened zirconia can be fabricated by using a cubic matrix with 20 to 50% tetragonal added (Harper, 2001).

2.4 Toughening Methods in Ceramics

Ceramics typically have low fracture toughness. Therefore in many engineering applications, we must increase the toughness. Some of the well established toughening mechanisms in ceramics with microcrystalline microstructure are: 1. Crack deflection or crack branching; 2. Toughening by a whisker bridging; 3. Crack bowing; 4. Metallic phase toughening and 5. Crack tip shielding by process zone activity, including microcrack toughening, transformation toughening or ductile yielding in the process zone (Mishra and Mukherjee, 2001). The following factors contribute to the fracture toughness of a composite:

- Volume fraction of reinforcement, fracture toughness increases for whisker reinforced ceramics as a function of increasing whisker content.
- Young's modulus of matrix and reinforcement. If a matrix is reinforced with high modulus, high-strength fibres, then more of the stress can be carried by the fibres.
- Strength of the matrix/reinforcement interface. In fibre-reinforced composites a strong interface can lead to transfer of the stress from the matrix to the fibres; a weak interface can lead to crack deflection (Carter and Norton, 2007).

2.4.1 Zirconia Toughened Alumina (ZTA) Composite

Zirconia toughened alumina, ZTA is a ceramic composite consisting of an alumina matrix embedded with either partially stabilized or unstabilized 0-50 wt% zirconia particles (Nevarez-Rascon et al., 2009). The addition of zirconia to alumina will enhance the basic mechanical properties; i.e. flexural strength and fracture toughness (De Aza et al., 2002). Hence, in order to explain such beneficial effects of adding zirconia particles to alumina, several mechanisms have been pinpointed, in all of them the second phase added being the main agent. First, transformation toughening as induced from the stress-induced transformation experienced by tetragonal zirconia particles when interacting with an advancing crack. Second, the effect of micro cracks intrinsically related to such transformation, which then promotes a toughening effect through the permanent dilatation and reduced modulus that they imply around the crack-tip. Third, the effect of internal stresses resulting from the differences in thermal expansion between the two phases, which set the alumina matrix under compressive residual stresses. On the other hand, the main toughening mechanisms operating in single phase alumina, i.e. crack bridging and crack deflection, seems to be of secondary importance in fine-grained ZTA_c (Casellas et al.,

1999). Figure 2.2 illustrates a transformation toughening mechanism in ZTAc. According to the literature, the optimum amount of zirconia should keep between 8-15 vol% to observe a compromise between improvements in fracture toughness, decrease in hardness and controlling grain size (Dey and Biswas, 2009, Rafferty et al., 2009).

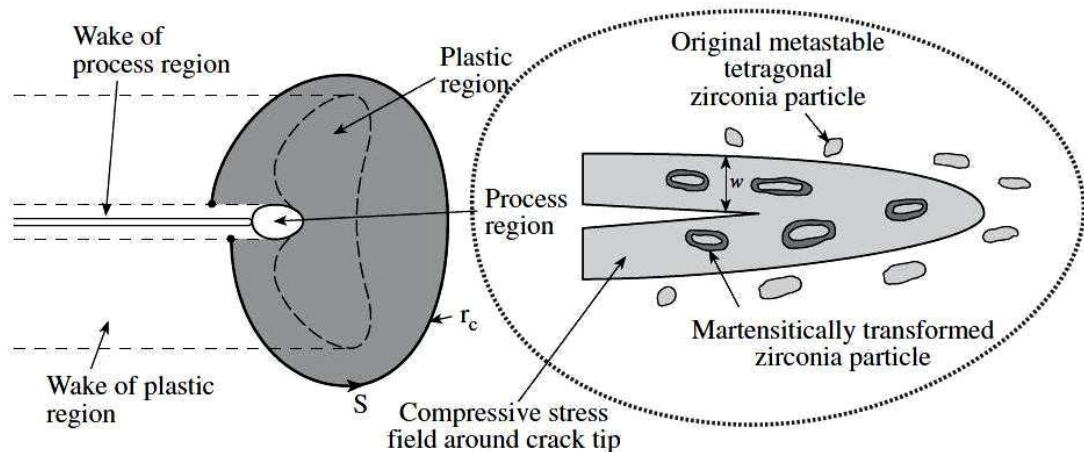


Figure 2.2 Illustration of transformation toughening in an alumina matrix containing ZrO_2 particles.

2.5 Ceramic Processing

The fundamental route to influence the ceramic microstructures is by controlling the ceramic processing. Most of the issues that are important for these processes are extensively treated in several books (Richardson, 1992; Ring, 1996). In general, ceramics are produced by using the following steps and the important parameters all discussed in relation to powder synthesis of raw material, consolidation, sintering and finishing. Ceramic powder preparation can, for instance, be realized by using wet-chemical processes, involving the co-precipitation of metal salts that are washed with water and alcohol. The starting powders

for ceramic processing have special demands, for especially particle size and morphology. These demands depend on the chosen consolidation route. A distinction can be made between various methods presented in Table 2.1.

Table 2.1 Some of basic forming methods

Casting; solidification; Suspension processing	Colloidal pressure filtration; Vacuum casting; pressure casting; slip casting; Gel casting; Tape casting; centrifugal casting; freeze casting Coating by: Sol-gel, Glaze, Electrophoretic, Thermal and plasma spray
Paste processing; deformation	Extrusion; Co-extrusion; Jiggering; roller tool forming; Plastic transfer pressing gel foaming; Suspension foaming; Molding(injection, compression); Roll forming
Dry powder pressing	Isostatic pressing; Combination pressing; Roll pressing
Post forming : creation shape by point, line or planer	Laminated object manufacture; Atom manipulation Ink jet printing Selective laser sintering; Stereo lithography

These are not all the potentials, but the most accustomed ones are listed. Consolidation by dry pressing is the most well-known method used for preparing ceramic pieces. For this method the particle morphology is of extreme importance. Irregularly shaped particles cause a lot of internal friction during pressing and they may result in high internal stresses or crack formation. Besides that the irregular shape may also be a cause of bad stacking of the powder during filling of the pressing mould. Using powder particles with a good morphology (preferably spherical and soft agglomerates) results in a good stacking process for dry pressing and a good compaction during pressing .The chance of creating defects by stacking faults or remainders of hard agglomerates is significantly

reduced. This is of course valid for composite ceramics as well. The presence of defects and inhomogeneities has a large negative effect on the properties of the ceramics in general. Examples are the final sintered density and mechanical properties such as hardness, toughness and strength.

Colloidal processing of ceramics is a preferred route to obtain near net shape components with a homogeneous and defect free structure. For suspension processing the particle shape is of less importance, since in most of these processes the powder particles are de-agglomerated before the consolidation step. Usually suspensions are made based on water and powder with some kind of stabiliser. Examples are electrostatic stabilisation and steric hindrance. The resulting suspensions are stable in the sense that they show limited or very slow sedimentation. These suspensions can be consolidated in various ways. The technique most frequently used in this thesis is pressure filtration. Paste processing methods usually involve not only stabilisers, but organic binders as well. Apart from the chosen consolidation route, it is of major importance for the homogeneity of the ceramic microstructure to prepare stable suspension of raw material. In the case of composite materials, the suspension preparation is the suitable step to create a homogeneous system. Dispersing and stabilising the system well means that the two phases are mixed properly and can be stacked in a very homogeneous way during the consolidation step. For both composites and single-phase ceramics the entire process can be used to control the presence of the defects or large voids.

Sintering is used for strengthening and densification of the ceramic bodies. During sintering usually three stages are identified. After consolidation, the powder particles are bonded by neck growth to give the ceramic body strength. This is followed by densification

where all large voids are removed and finally the grain will grow. Usually, the preference goes to the lowest sintering temperature possible. This is done for cost effective reasons and to keep the ceramic grain size as small as possible. Typical grain sizes for single-phase alumina and Y-TZP are 2 and 0.4 μm , respectively. Sintered ceramics are usually finished by machining and polishing to give them their final surface properties. By choosing a consolidation route that offers the possibility of near-net-shaping, it is possible to minimise the costs of the expensive post-treatments (Reed, 1988).

2.6 Colloidal Filtration Method

In batch wise pressure filtration, a suspension is separated into a green compact, and a pure filtrate liquid. The green cast is formed at a porous filter which is impermeable for the particles but permeable for the liquid. The driving force is a static pressure difference either accomplished by applying vacuum on the backside of the filter (vacuum casting) or by applying a high pressure on top of the suspension (pressure casting). The resistance to liquid flow in the filter is constant in pressure filtration, this in contrary to the process of slip casting in which a liquid front penetrates a porous filter (often plaster of Paris) due to capillary forces (Maarten Biesheuvel and Verweij, 2000, Michálková et al., 2010).

2.6.1 Particle Segregation during Filtration

When various particle types are suspended in a liquid or a gas, particles may segregate resulting in areas with different composition. This phenomenon can be observed in liquid fluidised beds, sedimentation in volcanic and in the processing of a suspension of ceramic particles to form a ceramic product. In the latter case, segregation leads to inhomogeneities in the products (casts) which are unacceptable when a homogeneous

composite should be made. Furthermore, segregation can cause cracks and warping as a result of differential shrinkage during subsequent drying and sintering. During in such a process segregation occurs in the consolidation step, when the particles in the suspension concentrate on the mould to form a cast. This occurs because the liquid is removed by drying or filtration or because the particles move through the liquid because of an external force. This consolidation mechanism is called sedimentation, and the sedimentation velocity depends on the forces acting on the particles.

According to the model presented by Maarten Biesheuvel (2000) the extent of segregation is neither influenced by the liquid viscosity nor by the particle sizes as long as the particle size ratio, and the hindrance factor power are constant and the mould permeability is high.

Segregation can be avoided by any of three methods:

1. A high suspension loading which reduces the cast formation time and lessens the hindrance factor for sedimentation.
2. Minimisation of the driving force for segregation $r_{p,1}^2(\rho_{p,1} - \rho_s) - r_{p,2}^2(\rho_{p,2} - \rho_s)$, which ρ_s is the density of suspension(kg/m³), $\rho_{p,i}$ is density of particles type i , kg/m³, $r_{p,i}$ the particle radius type i , m.
3. Use of a positive inter particle attraction (coagulation) which diminishes differential sedimentation and causes the particle packing to be more porous. For a more porous packing, the contribution of filtration increases and the cast formation time will decrease (Maarten Biesheuvel, 2000). However, the last solution is not useful when the homogeneous cast should be obtained.

2.6.2 Cast Formation Time

For pure filtration, cast formation time for a constant final cast thickness δ_c is calculated from Eq2.1 (Maarten Biesheuvel and Verweij, 2000).

$$t_c = \frac{45 \phi_c - \phi_s}{2\phi_s} \frac{\eta \delta_{dense}^3}{(1 - \phi_c)^3 r_p^2 \Delta P} \quad (2.1)$$

Which, Φ_c and Φ_s are cast concentration and suspension concentration respectively and $\Phi_c = 1 - \varepsilon$ which ε is the porosity of the cast, liquid viscosity η , Cast thickness δ_{dense} , pressure difference ΔP , particle radius r_p . For $\Phi_s \rightarrow 0$; t_c goes to infinity. No maximum of t_c be observed and t_c decreases monotonically with increasing Φ_s . Cast formation time increases for all values of Φ_s on increasing δ_c . One is often more interested in the cast thickness after densification δ_{dense} ($\delta_c \Phi_c$, assuming $\Phi_{c,dense} = 1$) instead of δ_c and cast resistance is considered as a negligible value.

For filtration with sedimentation in the same direction, cast formation time follows directly from Eq2.2 (Maarten Biesheuvel and Verweij, 2000):

$$t_c = \frac{\phi_c - \phi_s}{\phi_s \nu_0} \delta_c + X \ln \left(1 + \frac{\delta_c}{L_c R_f - X} \right), \quad (2.2)$$

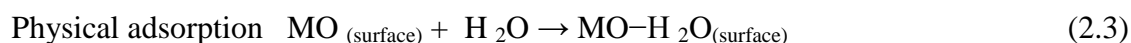
$$\text{and } X = \frac{\Delta P L_c}{\eta \nu_0}$$

L_c is cast permeability, R_f is the filter resistant, ν_c is sedimentation velocity

2.7 Colloidal suspension

A solution of table salt (NaCl) in water is called a true solution. The dissolved particles consist of single, hydrated ions and cannot be seen with the unaided eye. A suspension contains particles which you can often see them. Some examples of suspension

are flour in water and muddy water. In between the true solution and the suspension, there is the colloidal suspension or colloidal dispersion, the particles of which are bigger than ions, yet too small to be detected by an optical microscope. The particle size in a colloidal suspension lies between approximately 0.2 μ and 0.5 μ . Suspensions and colloidal dispersions differ from true solutions in that they are systems with more than one phase. In addition, in suspensions and dispersions the solid phase can be separated by filtration. Suspension can be filtered through filtering paper, colloidal suspension through an ultra filter. In colloidal suspension (named as a sol), liquid is the dispersion medium and a solid is dispersed, and they divided into two groups: lyophobic (Greek for liquid hating) and lyophilic (Greek for liquid loving) sols (Bormans, 2004). Water is a polar liquid and has a high dielectric constant and surface tension. Water can form the hydrogen bond with substances containing an $-OH$ or $-COOH$ group, and substances such as polymerized alcohols and carbohydrates dissolve in water if the molecule is not too big. The viscosity of water decreases significantly with increasing temperature. A polar liquid may be both physically and chemically adsorbed on the surface of dispersed oxide particles. For oxides such as Al_2O_3 , SiO_2 , ZrO_2 and CuO in water two kind of reaction have been suggested:



And



The polar hydroxyl ($-OH$) groups may cause the surface to attract and physically adsorb one to several additional layer of polar water molecules. The other liquids containing Methyl ($-CH_3$) and ethyl ($-C_2H_5$) molecular group are nonpolar. But hydroxyl ($-OH$), carboxyl ($-COOH$), sulfonate ($-SO_3^-$), sulfate ($-OSO_3^-$), ammonium ($-NH_4^+$), amino (NH_2) and polyoxyethylene ($-CH_2CH_2O-$) groups are polar in nature. A polar group

attracts polar liquid molecules and is called lyophilic group. A nonpolar group such as a hydrocarbon chain ($-C_xH_y$) is a lyophobic group. In aqueous system, these groups are often referred to as hydrophilic and hydrophobic group respectively.

Surfactants are molecules of a particular design which have one polar end and the other end that is nonpolar. They can be divided to nonionic, anionic and cationic. Nonionic surfactants do not ionize when dissolved in the liquid. Anionic surfactants have a relatively large lyophobic group that is commonly a long $-$ chain hydrocarbon and a negatively charged lyophilic group that is the surface $-$ active portion of the molecule. Anionic surfactants are widely used in industry. The driving force for the adsorption of a surfactant at a surface or interface is the reduction of the Gibbs free energy (ΔG) on its adsorption. When added to a polar liquid of high surface tension such as water, surfactant molecules will concentrate at the surface with the lyophilic end adsorbed in the polar liquid. An apparent concentration of only 0.01- 0.2 % may reduce the surface tension of the liquid very significantly and greatly improve the wetting of suspended solids by reducing the wetting angle. Accordingly, surfactants are often called wetting agents. Surfactant molecules may also improve the compatibility of the solid with the liquid medium when they are adsorbed at the interface and reduce liquid surface tension. When added along with an oxide powder into a nonpolar liquid, the surfactant will be adsorbed with the lyophilic end on the particle and the lyophobic end in the liquid. Polymer molecules with repeating ionizable group, called polyelectrolytes, which promote dispersion without necessarily reducing the surface tension or interfacial tension, are sometimes included in the category of surfactants. Then polyelectrolytes can also call deflocculants (Reed, 1995) .

2.8 The Stability of Colloidal Dispersions

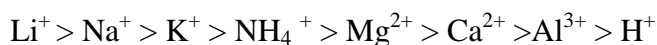
When dispersed particles in a lyophobic sol approach each other, two forces arise: Coulomb forces as a result of repelling force between particles with same charges and Van der Waals forces because of mass attraction between different particles. These forces are not large until the particles are very close to each other. The repulsion $E(R)$ energy and attraction $E(A)$ energy is plotted as functions of the distance between two particles. The total interaction energy of both particles is indicated by the curve $E(T)$. The curve $E(T)$ shows the energy threshold the particles have to overcome in order to be able to approach each other and thus form larger particles. When these enlarged particles have attained a certain size flocculation can take place, as a result the particles sink to the bottom and the suspension becomes unstable but vice versa the higher the energy threshold results the more stable suspension. The repulsion energy, and consequently the energy threshold, can be affected by adding an electrolyte to the suspension. This electrolyte mostly reduces the surface charges of the particles and the $E(R)$ curve moves to the left. This results in a $E(T)$ curve with a lower energy threshold (Bormans, 2004).

2.9 Stabilizing Method in Ceramic Suspensions

In most of the shaping technologies applied for ceramics, an indispensable condition is the preparation of an appropriate slip, i.e. a slurry or suspension (or possibly sol) without agglomerates or aggregates, exhibiting a rheological behaviour close to Newtonian in order to guarantee a homogenous microstructure of the formed body. Generally, there are two ways to avoid this flocculation and to stabilize the suspension, viz.

a. Sterical stabilization by polymers, which is dominant in suspensions with a high ion potential (e.g. in gypsum or cement suspensions), where the electrostatic stabilization is hindered

b. Electrostatic stabilization by electrolytes is the usual way of stabilizing ceramic suspensions. It is achieved by a sufficiently large electrostatic potential at the phase boundary (interface) of the colloidal micelle the so-called zeta-potential. In between there are dispersants that are functioning both via an electrostatic and a steric mechanism, which called polyelectrolytes and usually consist of a hydrocarbon chain and a polar ionic part (COO^- , SO_3^-). When the zeta-potential is sufficiently high, repulsive Coulomb forces are exceeding the attractive van der Waals forces, and therefore, the particles are repelled, do not flocculate and the suspension becomes stable. The value of the zeta-potential can be controlled by small changes in the composition of the suspension (by adding electrolytes or polyelectrolytes), and this value is then responsible for the rheological properties of the ceramic suspension. An increased zeta-potential results in a peptization, which reveals itself in a reduction of the viscosity (because of deflocculation) while a reduced zeta-potential, on the other hand, leads to agglomeration and an increase of apparent viscosity (and to coagulation). There are essentially two ways to enhance the zeta-potential: exchanging the ions adsorbed in the adsorption layer of the electrostatic double-layer while retaining the original value of the surface potential ψ , or/and raising the value of the surface potential ψ of the core of the particle. The ability of cations to disperse a given suspension containing agglomerates is described by the so-called Hofmeister series:



From this sequence, it can be concluded that alkali cations are the most effective in raising the zeta-potential. Their use, however, is undesirable, especially from the viewpoint of

further heat processing of biomaterials, because they lead to melt in a ceramic body, and the resulting inhomogeneities (e.g. glassy boundary phases or recrystallization products) dramatically decrease the mechanical strength. Furthermore, they may possibly affect the biocompatibility of the materials. Therefore it is not advisable to apply an exchange adsorption of alkali ions in order to achieve stabilization of the slurry. Thus for the electrostatic stabilization of advanced ceramics suspensions only the second route for enhancing the zeta-potential is feasible (enhancing the surface potential ψ by alkali-free electrolytes or polyelectrolytes) (KUNEŠ et al., 2000).

Some of the dispersants which have been used to disperse ceramic powders consist of alumina and zirconia are Alu-minon, ammonium polyacrylate, Tiron, diammonium citrate, 2-propenoic acid, polymethacrylic acid, polyethyleneimine and Triton-X114. Greenwood and Kendall (1999) have complete a comprehensive study using 14 different reagents for dispersing zirconia.

2.9.1 Dolapix CE 64

A carbonic acid-based polyelectrolyte, free from alkali, according to the manufacturer, the dispersant possesses bivalent groups, and is characterized by adsorption on the particle surfaces and complete dissociation at pH above 8.5 (Gaydardzhiev, 2006 & Albano et al, 2002). The chemical structure is given in Figure 3.2 (Mei et al, 2001 & Prakash Rao et al, 2007)

It has been described earlier (Dakskobler et al, 2001) that Dolapix CE 64 is an ethanol aminic salt of citric acid.

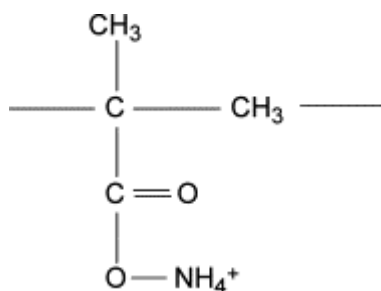


Figure 2.3 Chemical structure of the dispersant

2.9.2 Tiron

4,5 -dihydroxy-1,3-benzenedisulfonic acid, disodium salt, commercially known as Tiron. Tiron is a feeble tetraprotic acid, resultant of two hydroxylic and two sulfonic groups attached to a benzene ring with low molecular weight. The sulfonic acid sites easily give up their protons, resulting in very low pK_{a1} and pK_{a2} values, usually not reported ; pK values associated to the hydroxylic acid sites are $pK_{a3} = 7.7$ and $pK_{a4} = 12.6$. It is a proficient complexing agent for several metallic cations, which enhances its adsorption ability onto particles' surfaces of the metal oxides. Additionally, the ionizable sulfonate groups lead to negative charge development and Na^+ cations coordinate around complexes supporting their stabilization. Hence, particle's surface becomes highly charged and electric double layer repulsion increases, creating a high repulsive potential between the particles and improving their dispersion capability.

Namely, Tiron is well known as an extremely effective anionic dispersant in aqueous media for Al_2O_3 (Gulicovski et al., 2008), ZrO_2 (Briscoe et al., 1998, Moghadas et al., 2011) Figure 2.4 presents schematic structure for Tiron(Guedes et al., 2009)

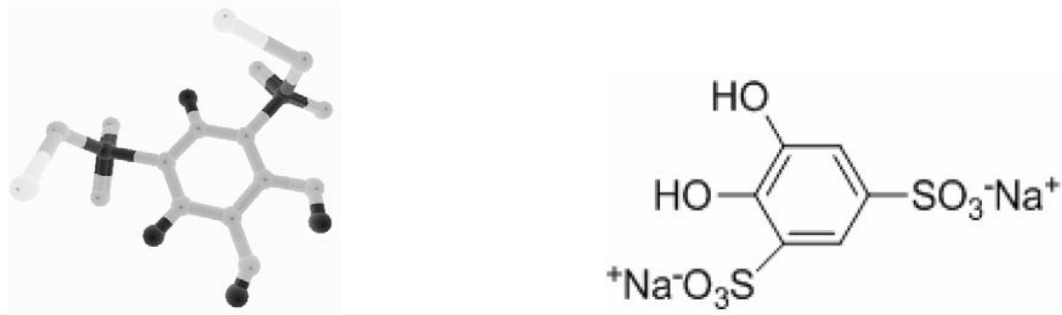


Figure 2.4 Tiron (a) structural formula and (b) 3D view

2.10 Density and Porosity Measurements

Density measurements were performed according to the Archimedes technique in mercury for green body and in water for sintered bodies. The Archimedes theorem explains that all bodies immersed in a fluid will be buoyed up by a force equal to the weight of the fluid that displaced. Densities were calculated from Equation 3.2:

$$\rho_1 = \frac{W_1}{W_1 - W_2} \rho_0 \quad (2.2)$$

Where ρ_1 is the density of solid body, W_1 is the weight of the solid body in air; W_2 is the weight of the solid body when it is immersed in distilled water. The ρ_0 is the density of mercury or water, 13.594 and 0.9970 g/cm³ respectively at 25 °C. The theoretical density was measured by the rule of density in composites from Equation 3.3:

$$\rho_t = \rho_1 f_1 + \rho_2 f_2 + \dots + \rho_n f_n \quad (2.3)$$

Which f_1, f_2, \dots, f_n are the volume fractions of the elements in the composite which were calculated from equation (3.4):

$$f_1 = \frac{m_1 \rho_2 \dots \rho_{n-1} \rho_n}{m_1 \rho_2 \dots \rho_{n-1} \rho_n + m_2 \rho_1 \dots \rho_{n-1} \rho_n + \dots + m_n \rho_1 \rho_2 \dots \rho_{n-1}} \quad (2.4)$$

$\rho_1, \rho_2, \dots, \rho_{n-1}, \rho_n$ are the density of different elements of composite.

And $m_1, m_2, \dots, m_{n-1}, m_n$ are the weight fraction of different elements

Relatively density, ρ_r simply is calculated through equation (3.5):

$$\rho_r = \frac{\rho}{\rho_t} \cdot 100 \quad (3.5)$$

Other than the density sometimes we need to measure the porosity of sintered samples (closed and open), when the porosity is close to zero, the compound is dense and the density is almost close to the theoretical. The relatively closed porosity of ceramic component is measured by follow equations.

$$\phi_{closed} = 100 - \rho_{r,1} \quad (2.6)$$

The $\rho_{r,1}$ is the relatively density when the liquid is water or an absorbable liquid, and to measure the volume of open and closed porosity.

$$\phi_t = 100 - \rho_{r,2} \quad (3.7)$$

ϕ_t is the total porosity include closed and open, $\rho_{r,2}$ is the relatively density of compound when the used liquid is mercury or any other non-absorbable liquid.

2.11 Firing

The green products are heated below the melting point in a furnace to develop the desired micro structure and properties.

This process, called firing, proceeds in three stages: I) reactions preliminary to sintering; II) sintering, which starts when the temperature is one-half to two-third of the melting temperature, and it contain densification and shrinkage and III) cooling, which may include thermal and chemical annealing. Sintering, is defined as a complex procedure consists of many transport mechanisms for densification of powder and microstructure improvement. Powder characteristics, including composition, agglomeration tendency, and particle size distribution, sintering methods and forming technique all have a considerable role in sintering behavior of materials.

In Al_2O_3 and 3Y-TZP compacts the solid-state sintering could be describe the particles behavior during sintering. The driving force for the sintering has its origin in the reduction in the total free energy ΔG_T of the system,

$$\Delta G_T = \Delta G_V + \Delta G_b + \Delta G_s \quad (3.8)$$

Where ΔG_v , ΔG_b and ΔG_s represent the change in free energy associated with the volume, boundaries and surfaces of the grains, respectively. The major driving force in solid-load sintering is $\Delta G_s = \gamma_s \Delta A_s$ (Reed, 1995). In solid state sintering, material is transported by diffusion, when the materials of the separate particles diffuse to the neighboring particles. In general during sintering three stages were recognized: (1) neck forms; (2) neck growth and make a continuous network of pores; (3) pore channels destroyed and grain coarsening happened (Aminzare et al., 2011).

Conditions such as time, temperature and atmosphere are crucial in a sintering procedure; hence, it has been investigated widely to optimize these parameters. According to the experimental study (Lance et al., 2004) and also different simulation such as kinetic field diagram or rate controlled sintering (RCS) (Raether and Schulze Horn, 2009) and master sintering curve (MSC) (Mazaheri et al., 2009) and (Aminzare et al., 2010) we are able to predict and optimize the best temperature and time for ZTA (15 wt% 3Y-TZP) to obtain near full density with small grain size.

2.12 Mechanical Properties

The strength of ceramics is affected by many factors, such as composition, microstructure (grain size, phase distribution, pores and cracks) and the surface conditions which they are

also influenced by raw material, processing, firing and even finishing. In addition, temperature and environment condition is considerable factors.

2.12.1 Hardness

The hardness test is available as a relatively simple alternative to the tensile test. The resistance of the material to indentation is a qualitative indication of its strength. The hardness of a material is its resistance to the formation of a permanent surface impression by an indenter. It will also define as resistance of a material to deformation, scratching, and erosion. We measure the actual area of the impression. The hardness is determined by dividing the applied force, F , by projected area: a^2 . The hardness is then:

$$H = F / a^2 \quad (2.5)$$

α is a numerical factor that depends on the shape of the indenter. The processes that happen under the indenter tip can be quite complex. We often see a deviation from what is called “Hertzian” behaviour where the indentation stress is proportional to the indentation strain. The geometry of the indenter tip and the crystal orientation will affect the hardness. There are many different hardness tests, and each gives a different number. The indenter can be either rounded or pointed and is made of material much harder than the test piece. The deviation is due to plasticity beneath the indenter as illustrated in Figure 2.5.

2.12.2 Fracture Toughness

The fracture toughness of a material, in simplest terms, can be described as the stress required to initiate a crack when a stress is applied. In that sense ceramics are not as tough as metals and alloys. There are several techniques to determine K_{IC} for a ceramic. The two main approaches are to use indentation or bending.

The use of indentation techniques for determining K_{IC} has been the subject of many studies since being introduced by Lawn and Wilshaw (1975) and Anstis et al (1981) The critical stress intensity factor is obtained by assuming that the applied stress intensity caused by the load is equal to the critical stress intensity for crack propagation.

$$K_{IC} = \eta \frac{\sqrt{E}}{H} \frac{F}{C^3/2} \quad (2.6)$$

Where, η is a geometric factor and is a dimensionless constant, which for alumina based ceramics has an average value of 0.016 ± 0.004 , and for Zirconia based ceramics it measured to be 0.025 ± 0.002 for zirconia based composites (Casellas et al., 1999).

E the Young's modulus of elasticity, H is the hardness, F is the indentation load, and C is the indentation radial crack half length of the cracks parallel to the layers at the surface (Carter and Norton, 2007). The basic idea is illustrated in Figure 2.5.

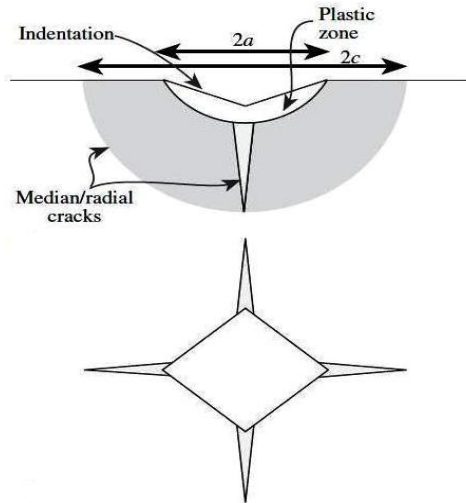


Figure 2.5 Cracks at an indent allow determination of K_{IC} .

For $c/a > 2.5$ (present study), where c is the crack length and a the half diagonal length of the indentation impression, is calculated using the following equation (Meza and Chaves, 2003, Nevarez-Rascon et al., 2009) :

$$K_{IC} = 0.0752 \cdot P \cdot c^{3/2} \quad (2.7)$$

Where K_{IC} is the fracture toughness, P the load and c the crack length.

2.13 Wear and friction

Wear resistance is not a property that can just be described for a material specifically. It is influenced by many parameters determined by both the system and the material that are used. Since wear is primarily a system property (also depending on load, velocity, temperature), it is usually described in terms of a specific wear rate, k_w :

$$K_w = \frac{V_w}{F \cdot s} \frac{mm^3}{N \cdot m} \quad (2.8)$$

Here, V_w is the wear volume of the examined sample [mm^3], F is the applied load on the configuration [N] and s is the sliding distance [m]. All materials that tested on their

tribological behaviour are characterized by this parameter. This parameter represents wear as a function of system conditions only.

The other important issue in tribological studies of materials is friction. Friction, occurring between two surfaces in contact with each other, can be the cause of several other features influencing wear of materials. The coefficient of friction, f , is defined as the ratio between the measured friction force, F_F , and the applied normal force, F_N :

$$f = \frac{F_F}{F_N} \quad (2.9)$$

Frictional heating is usually the most important feature influencing wear. Due to the relatively low thermal conductivity of most oxide ceramics, the contacting materials will be heated. The thermal aspects influence the performance or efficiency of the system. For instance, the presence of temperature gradients, may propagate crack formation in the contacting surfaces, which can cause severe wear (Wang and Hsu, 1996).

2.14 Wear in ceramics

For ceramics, there is couple of specific wear phenomena by which material removal takes place. Ceramics show fracture processes that are typical for brittle materials. Micro cracking is the largest cause of wear in ceramics, but plastic deformation can occur in fine-grained materials (on a scale < 1 mm) or when locally temperatures become extremely high. Another important feature in wear of ceramics is the transition from mild to severe wear at certain loads or velocities. In general, this transition is usually noticed by a change in the way wear takes place; the wear phenomenon changes from plastic deformation to brittle fracture and micro cracking. The transition point is found where the

measured wear volume shows a sudden increase in time. The main reason for this transition to occur is the increased material pull-out at higher loads or velocities (microcracking and delamination) or during prolonged sliding. This material pull-out causes a larger contribution of abrasion to the wear process. The application of ceramics under extreme loading or velocity conditions still suffer from this transition, but under unlubricated conditions the value for the transition load for ceramics is lower than for metals. Therefore, it is necessary to develop ceramic materials with a high transition load.

The wear (transition) mechanisms that occur are predominantly dependent on the tribological contact stress in the material (mainly resulting from the applied load). Low contact stresses result in wear by plastic deformation. In high contact stress, cracks are formed and at an acute point, severe wear processes develop. This transition point is related to the point where the tribological stress exceeds the critical crack or fracture stress. This can happen at both a local, microscopic and macroscopic scale. Demonstrations of feasibility of various models for wear volume predictions were found in literature (Wang and Hsu, 1996). Most of these models are based on the fact that when the maximum tensile strength, σ_{max} , exceeds the value for the critical stress, σ_D , in a material, cracks appear on the surface. For wear volume predictions, the normalised threshold stress, (σ_{max}/σ_D) , is of particular interest. Theoretically this value should equal 1, but due to surface cracks present before wear the value for s_D is usually significantly lower in polycrystalline ceramics. Reported transition phenomena for the self-mating wear of MgO stabilised zirconia. These transitions were defined as stress-induced surface fatigue transitions (inter-granular microcracking), humidity-dependent protective physical and chemically induced layer film formation, pressure-dependent phase transformations and tribo-oxidation-induced wear-

reducing or wear-accelerating transitions, mainly indicating the extremely difficulty of tribological research in relation to material properties and operating condition.

2.15 Solid-state lubrication

Friction reduction for ceramic couples is an important issue in ceramic engineering. For the widest range of possible applications of ceramics, the ceramics must have low friction at high temperatures and preferably under unlubricated conditions. Normally, lubrication can be performed using water, oils, greases and solids. If lubrication is necessary for high temperatures, the possibilities of available materials are rapidly limited to solid-state lubricants. They have a finite lifetime as a functional material, since it is consumed during the process. However if we incorporate lubricants in a ceramic matrix material, a self-supplying lubricating phase will be possibly created. An example of the use of solid-state lubricants is given by Wang et al. They describe friction and wear of PSZ ceramics lubricated by copper or copper oxide. They succeed in lowering the friction from 0.4 to 0.14 under varying loads (18-80 N) and velocities (0.01-0.1 m/s) (Wang et al., 1993). They describe how the coefficient of friction relates with the properties of the solid lubricating film. Then the coefficient of friction is explained as the ratio between the shear strength of the lubricant film, the true contact area and the contact load. Kerkwijk et al confirmed a fluctuating influence of several soft oxides on friction, wear and microstructure of α -Al₂O₃ and Y-TZP composites. The most valuable result was found where the coefficient of friction effectively dropped off in conjunction with a good wear rate of 10–8 mm³/Nm. Y-TZP- CuO showed a friction reduction of about 40% (0.70 - 0.43), in sliding against alumina balls (Kerkwijk et al., 2004).

CHAPTER 3 RESEARCH EXPERIMENTAL DESIGN

3.1 Introduction

This section presents the information about particular material consumed in this work, production process and preparation of substances for characterizing mechanical properties. It explains the applying methods for measuring different properties in order to give a clear feature of using the colloidal method. It also includes a short summary about the equipments in use and brief instruction for collecting data with high accuracy.

It is considered to provide samples by colloidal filtration and stages of production as shown in the following flowchart.

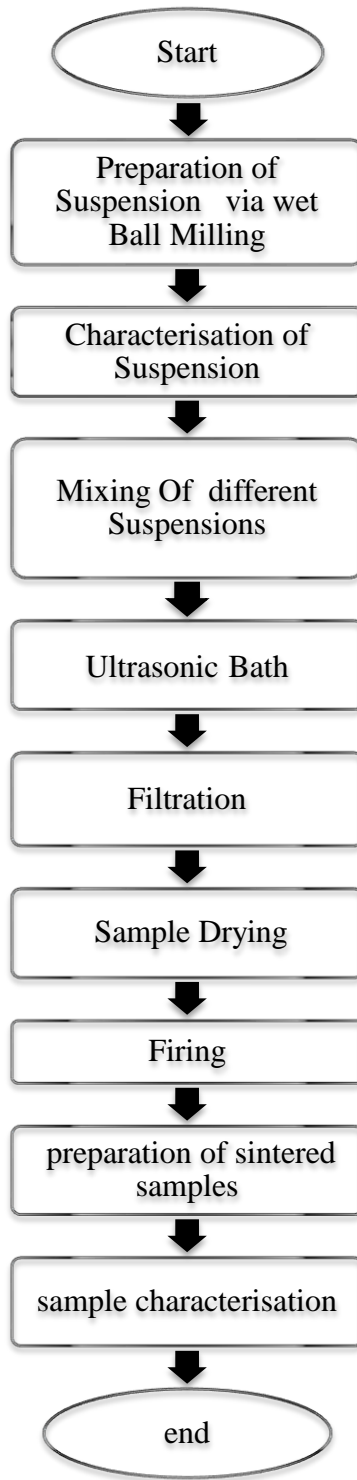


Figure 3.1 production procedure

3.2 Material

High purity alumina (α -Al₂O₃, Alfa Aesar, 99.95), 3 mol% yttria-stabilized zirconia (ZrO₂, Sigma Aldrich, 5.3wt% Y₂O₃ thereafter abridged as 3Y-TZP), CuO and MgO (Sigma Aldrich, nano powder) were used as starting powders. Their characteristics are presented in Table 3.1.

Table 3.1 Properties of starting material.

Powder	Average particle size	Y ₂ O ₃ (Mol %)	Melting Point (°C)	Surface area (m ² /g)	Molecular Weight (g/mol)
α -Al ₂ O ₃ 99.95%	0.3-0.49 μ m	-	2045	7-9	123.22
ZrO ₂ 99.5%	0.5 μ m	3	2600	6.9	101.96
CuO	30-50nm	-	1326	13	79.54
MgO	100nm	-	2852	11	40.30

Dolapix CE64 (Zschimmer and Schwarz GmbH, Germany) and Tiron (Aldrich) were added for dispersing of suspensions and their characteristic are given in table 3.2.

Table 3.2 Properties of two different dispersants.

Material	Molecular formula	Molecular weight (g/mol)	Appearance	pH	Density (g/cm ³)	Viscosity (Pa.s)
Dolapix CE64	Carbonic acid based poly electrolyte	320	Yellowish, liquid	7	1.2	0.578(20°C)
Tiron	C ₆ H ₄ Na ₂ O ₈ S ₂ ·H ₂ O	332.20	Light, tan powder,	3-3.5 (1 wt% in water)	Soluble in water but Solubility in water depend on the pH	

3.3 Preparation of Single phase suspension

To prepare stable suspension of the oxides, first appropriate amount of as-received powder of α -Al₂O₃, 3Y-TZP, CuO and MgO were separately weighted (using Kshida Shinko weighting machine with up to 0.001g accuracy) then were poured in the small polyethylene containers which had been filled with a proper amount of distilled water and dispersant. Dispersant first was introduced to water and mixed for 15 minutes by a magnetic stirrer. Zirconia balls (Retch, Germany, diameter: 10mm) added in to the polyethylene container and mixing process was continued by means of horizontal ball mill (Pascall engineering). The ratio of the balls mass to the powders was 5:1. However, higher material loading are often used when dispersing agglomerates and mixing is the primary objectives. The polyethylene container was placed inside the ceramic jar of the horizontal ball mill (or any other jar which is adjustable on the mill). The mill was operated in 300 rpm, while the rotary velocity translated to jar is lower and should be lesser than critical angular frequency ($\omega = 0.5R^{-1/2}$, R is the radius of the jar) to avoid causing centrifuging.

Ball milling will process for at least 16 hours to disperse the hard agglomerates and aggregates (Reed, 1995).

Table 3.3 Characteristic of initial single phase suspension.

suspension	Solid powder (g)	Water (g)	Mixing time	Wt% solid load	Dolapix(g) Tiron(g)	pH
(1)- Al ₂ O ₃ 66.6 wt%	10	5	16	66.6	0.04	9.31
					0.05	9.1
(2)- 3Y-TZP 33.3wt%	5	10	16	33.3	0.02	8.2
					0.025	8.05
(3)- CuO 5 wt%	0.5	9.5	4	5	0.004	9.32
					0.005	9.35
(4)- MgO 5 wt%	0.5	9.5	4	5	0.004	10.83
					0.005	10.76

3.4 Zeta Potential, pH and Viscosity

In order to find out the practical pH area to prepare stable suspension of Al₂O₃, 3Y-TZP, MgO and CuO as well as their mixture it is necessary to do a primary study on potential zeta point and viscosity.

Zeta-potential measurements of dilute slurry of different oxides (0.05 wt %) were done using a Zeta-Meter, Nano-series (Malvern model ZEN3600 instrument, particle size range: 3nm to 10µm). Dilute suspension of oxides separately was conditioned overnight in 0.01 M % KNO₃ solution in a magnetic stirrer. The purpose of sample preparation is to save the existing state of the surface during the process of dilution with regard to the pH, total ionic concentration of the system and Concentration of any surfactants or polymers present. The measurement were done in the pH range 3 to 12.5 by employing auto titrator MPT-2, using nitric acid for acidic adjustment and ammonium hydroxide for basic

adjustment. For each sample, three values of zeta-potential were measured and an average was reported.

The pH of diluted and concentrated slurry of oxides and their mixture were measured by using pH meter (Eutech Instrument with glass-body pH electrode suitable for high viscose samples). The potential at the slipping plane is known as zeta-potential and it has repeatedly been used for the discussion of colloid stability, and its value is considered useful in relative to the electrical double layer.

Zeta potential is measured using a combination of the measurement techniques: Electrophoresis and Laser Doppler Velocimetry, sometimes called Laser Doppler Electrophoresis. This method measures how fast a particle moves in a liquid when an electric field is applied. The movement of charged colloidal particles or polyelectrolytes, immersed in a liquid, under the influence of an external electric field commonly referred to electrophoretic mobility, U_E ($m^2 V^{-1} s^{-1}$) which is the magnitude of the velocity divided by the magnitude of the electric field strength. The mobility is counted positive if the particles move toward lower potential (negative electrode) and negative in the opposite case (Delgado et al., 2007, Lee and Speyer, 2002).

With this knowledge, we can obtain the zeta potential of the particle by application of the Henry equation.

$$U_E = \frac{2Z\epsilon f(K_a)}{3\mu} \quad (3.1)$$

Z: Zeta potential; U_E : Electrophoretic mobility; ϵ : Dielectric constant; μ : Viscosity.

$f(K_a)$: Henry's function (in aqueous media and moderate electrolyte concentration is 1.5, and is referred to as the Smoluchowski approximation). The viscosities of suspensions with solid loadings up to 70 wt% and dispersant concentrations between 0 and 1 wt% solids

were measured using a sine-wave vibro viscometer with wide measurement range 0.3 mPa·s - 10,000 mPa·s (Model SV-10, A&D Instruments). Sine-wave Vibro Viscometer series measures viscosity by detecting the driving electric current necessary to resonate the two sensor plates at a constant frequency of 30 Hz and amplitude of less than 1mm. Figure 3.2 shows a picture of the viscometer used in this work.

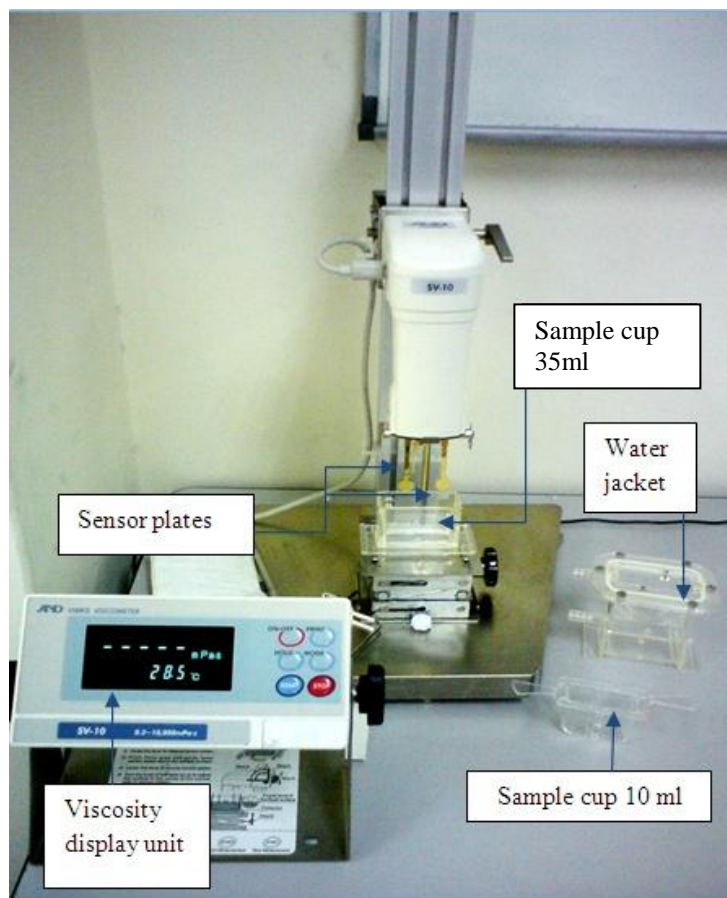


Figure 3.2 SV-10 series vibro viscometers.

3.5 Preparation of suspension of different Oxides

In this stage, the stable slurries of Al_2O_3 and 3Y-TZP were mixed with weight ratio 85/15 and milled for 4 hours then viscosity and pH measurements were done for the mixed suspension. In order to prepare ZTA with doped magnesia or copper (II) oxide, the small

amount of prepared suspension of the magnesia and/or copper (II) oxide was added and mixed in ball mill for 2 hours. All measurements were done with respect to the density of slurries and according to the proportion of each oxide in the final substances.

Table 3.4 Characteristic of mixed suspension of different Oxides

Suspension	Al ₂ O ₃ %	ZrO ₂ %	MgO%	CuO%	% wt solid	pH in presence of Dolapix (0.4 wt%) Tiron (0.5 wt %)	Viscosity(mPa.s) Dolapix (0.4wt %) Tiron(0.5 wt%)
(5)Al ₂ O ₃ and 3Y-TZP	85	15	-	-	60	9.1 9.2	16 9
(6)Al ₂ O ₃ and 3Y-TZP	85	15	-	-	50	8.6 8.6	6 3
(7)Al ₂ O ₃ and 3Y-TZP with MgO	84.5	15	0.5	-	50	9.36→11 9.8→10.5	10 8
(8) Al ₂ O ₃ and 3Y-TZP with CuO	84	15	-	1	50	9.6 8.65	7 4
(9)Al ₂ O ₃ and 3Y-TZP with MgO and CuO	84.85	15	0.05	0.1	50	9.14→11 9.3→10.5	20 14

For instance, 84.85wt% alumina, 15 wt% stabilized zirconia, 0.1 wt% copper (II) oxide and 0.05 wt% magnesia need to mix for preparing suspension for ZTA composite with MgO and CuO. To prevent using of any agglomerated slurry the rheological properties of slurries were checked in each step, subsequently, the containers were placed in an ultrasonic bath (Starsonic 90, Italy) for 15 minutes, at a frequency of about 20-30 kHz. Table 3.4 presents basic information about mixed Al₂O₃and 3Y-TZP suspension.

3.6 Filtration Procedure

The glass filtration equipment, 15 mm diameter was used for consolidation of suspension (Figure 3.3).

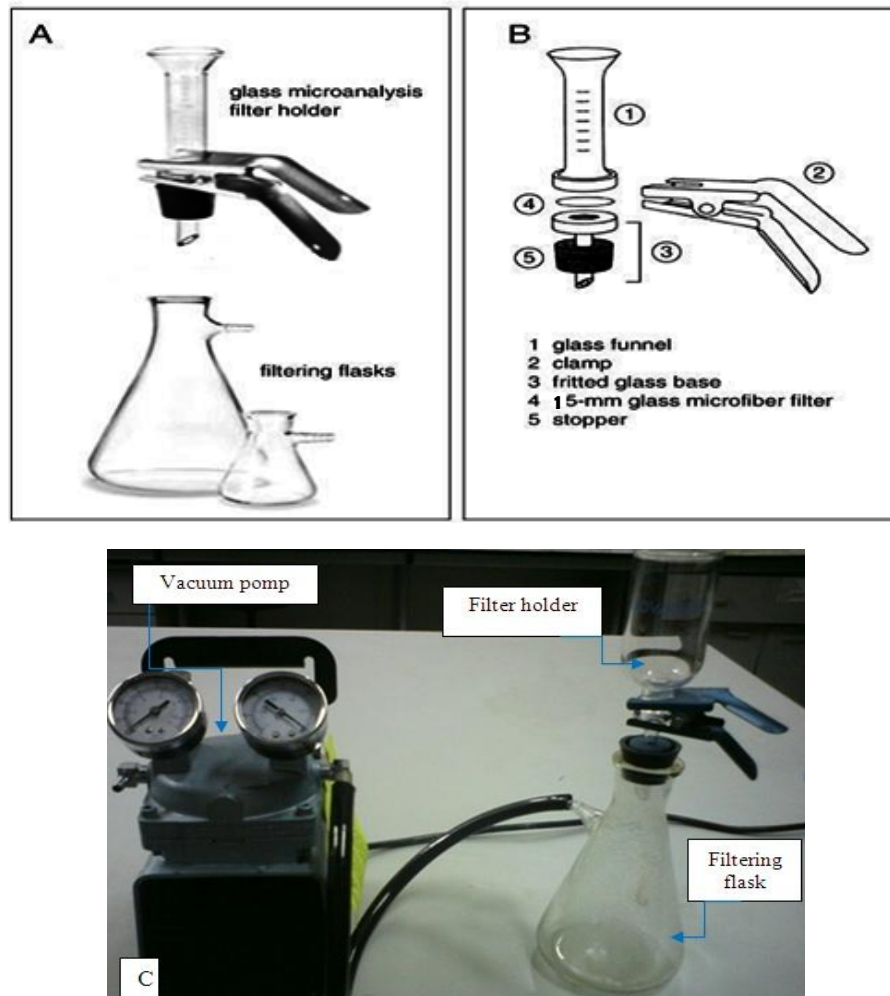


Figure 3.3 A and B: general part of a filtration equipment; C: The glass filter used in this work.

The membrane was cellulose nitrate filter with a pore size of $0.45\mu\text{m}$ (Whatman GmbH). The suspension surface remained in contact with the atmosphere while the driving force for the filtration was created by a vacuum at the other side of the membrane filter.

Castings were performed under vacuum pressure of 590 mmHg at 25 °C for 15 to 45 minutes.

3.7 Characterization of Green samples

To determine the sintering shrinkage and weight loss the thickness and diameter of samples were measured before and after sintering by means of vernier scale and also dry samples were weight by balance.

3.8 Sintering

The green bodies obtained by the filtration were sintered in a chamber furnace. The Lenton furnace has a maximum operating temperature of 1600°C, and this furnace is an electrical resistance furnace in which a current carrying resistor provides the source of heat. The furnace has a double skin construction which allows natural air convection to maintain a cool outer case. Firing procedure for all components in this project started with a heating rate of 10 °C/min to 1000 °C (the lower heating rate results big grain size (Aminzare et al., 2011) and higher heating rate could end crack in samples), and then continued with 5 °C/min to 1550°C. Sintering was completed with dwelling in this temperature for 2 h under air atmosphere, subsequently the cooling takes place in a shouted down furnace. In order to avoid any contamination and minimize damage in the green compacts during sintering, samples were placed in high-purity alumina crucibles.

3.9 Sample Preparation

Before microstructure analysis, the sintered specimens needed to be cut (here only for cross-section study), ground, polished and thermally etched. Sintered samples were cross-

sectioned by an Abrasive Cutter machine. In general ceramic materials are very feeble in tension; special care must be taken in choosing proper cutting processes. During cutting the coolant flow rate must be controlled and to avoid vibration the cutting rate must be kept low. It is also worth noting that fixing and holding of sample in the Abrasive Cutter tool needed some precautions. Very tight fastening would damage the surface and break the ceramic.

Appropriate surfaces were ground using polishing machine (Struers, The terga system) apparatus by the SiC abrasive papers, Struers grit 500, 800, 1000, 1200 and then polished with MD-Polishing cloths (MD-pan: Impregnated, non-woven technical textile, MD-Dur: Satin woven natural silk, MD-Chen: Porous neoprene), and stable diamond suspension with particle size of 9 μm , 3 μm and 1 μm and suspensions of 0.5 μm alumina particles were used with the polishing cloths respectively. Thermal etching is commonly apply in ceramics to display the microstructure of ceramics which mostly present difficulties in perceiving micro structural features by chemical etching Thermal etching involves heating the polished specimens at a temperature few hounded below the sintering temperature for 15 to 60 min(Carter and Norton, 2007) (Lorenzo-Martin et al., 2009). The micro structural features are revealed in thermal etching by the grooving of the grain boundaries and phase boundaries as a result of surface and grain boundary diffusion. The cross-sectioned and polished specimens were thermally etched at a rate of 5°C/min and held at 1350 °C for 30 minutes in the Lenton Furnace. The final average surface roughness of samples was around 0.1 μm and it was measured by using of Surface Roughness Tester TR200/210/220 (measuring range for R_a : 0.025-12.5 μm)

For polishing process and also for applying indentation for Vickers hardness it is necessary to mount samples with epoxy (Struers, epo fix resin and epo fix hardner, mixing

ratio 25/3 by weight and 15/2 by volume, curing time is 12 hours). Therefore, the samples were prepared for type's characterizations test such as SEM, Vickers Hardness and so on.

3.10 Sample Characterization

3.10.1 Vickers Hardness (HV) and fracture toughness

Mechanical properties were investigated through indentation method using standard indenter, Frank 532. The hardness is calculated with the below formula:

$$HV = \frac{F}{A} \approx 1.8544 \frac{F}{d^2} \quad (3.9)$$

Where F is the force applied to the diamond, A is the area of the indentation and d is the average value of the diagonals of the imprint created by the indentations.

The hardness test instrument used is the Vickers hardness Model Mitutoyo, AVK-C2. A diamond indenter in the form of a square-based pyramid with an angle of 136° between with the opposite faces at the vertex is pressed into the surface of the test piece using a prescribed force F . After the force has been removed, the diagonal lengths of the indentation d_1 and d_2 are measured. The test force is maintained for 15 s and 10 kg loads were applied by the indenter to the sample's surface. The results were obtained and dimension of the crack that cratered on the surface were recorded for measuring the indentation fracture toughness. More details are in ASTM standard C1327-97 which is test method for Vickers indentation hardness of advanced ceramics.

3.10.2 X-Ray Analysis

Fingerprint characterizations of as-received powder of raw materials and sintered samples after thermal etchings were determined using a Philips X'pert MPD PW3040 XRD

using $\text{CuK}\alpha$ radiation at 1.54056 Å X-ray wavelengths. The samples were scanned from 10° to 80° 2θ angle at a step size of 0.20 and a count time of 1.5 at each step.

Diffraction patterns occur as a result of scattered X-radiation by atoms whose spacing is comparable in magnitude to the wavelength of the radiation. When an incident X-ray beam with wavelength λ strikes on two parallel planes of atoms at θ angle, it will be diffracted by atoms in the planes A and B which are separated by the d spacing. Figure 3.4 is a simple view of X-ray diffraction. The diffracted beams will be completely in phase if the path length is equal to a whole integer of the wavelength. The condition of constructive diffracted rays is governed by Bragg's Law:

$$n\lambda = 2d \sin \theta \quad (3.10)$$

Bragg's law relates the X-ray wavelength and inters atomic spacing to the angle of the diffracted beam. Variations in the θ angle from 10° to 80° during scanning of a polycrystalline sample will satisfy the Bragg's law conditions by virtue of its many different d spacing. The bulk sample's surfaces and cross-sections are cleaned with alcohol and placed into the sample chamber diffractometer.

3.10.3 Scanning Electron Microscope (SEM)

The microstructures of different components were studied using a Scanning Electron Microscope (SEM). The aim of the test was to obtain representative images of surface and cross-section of prepared compositions to investigate the homogeneity of samples and also to measure the grain size. It is necessary to prepare the samples to carry out and to obtain a micrographic study. A Philips XL30 (SEM-EDX) was employed to investigate the microstructure and elemental composition of the sample in various layers.

Philips XL30 (SEM-EDX) has a high magnification in excess of 200,000 times and a resolution of 3.5 nm at an accelerating voltage of 30 kV. Basically, the manner of operation for the SEM to study the surface is to bombard it with electrons, and then the reflection is measured. Free electrons are created when the tungsten cathode is heated. Then, the electron accelerated towards a positive electrode. On the edge of the anode, the electrons; velocity has increased to their maximum speed and the width of the beam is between 5 and 10 micrometers. According to the modern physics, when passing the anode, the electrons show wave properties. A condenser is used to focus the electron beam. The coils are used to see the whole sample. The electron beam continues past the diaphragm, which controls the distance from the sample studied. Thus, it can be to representative image. The electron capture detector reflectivity depending on the direction and intensity, the image is showed a clearer or darker point.

The samples were provided for characterizations, the surface of cross-sectioned samples was covered with a very thin layer of gold, and this is made to reveal the grain surface and boundaries of them. So that, the SEM can captures the reflected electrons.

3.11 Wearing test

Dry-sliding wear tests on ceramic discs were performed at room temperature on pin-on-disc tribometer (Recipratory friction and wear monitor, TR261). Commercially available 10 mm zirconia bearing balls (grade 10, Aldrich) were used as pin material. The geometry of the test set-up, prepared specimen and ball inside holder is shown in Figure 3.5. a and b

The sliding velocity in the contact was set at 0.1 m/s. A constant force, F , of 10 N was applied resulting in an initial mean Hertzian contact pressure of 1130 MPa. Dry sliding

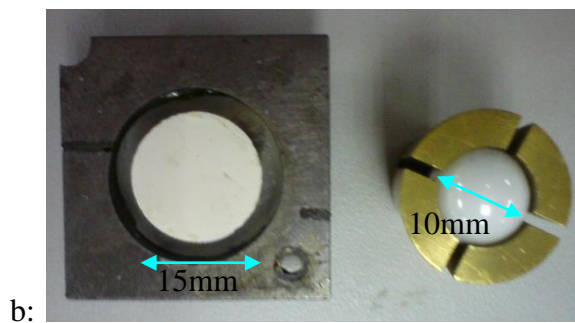
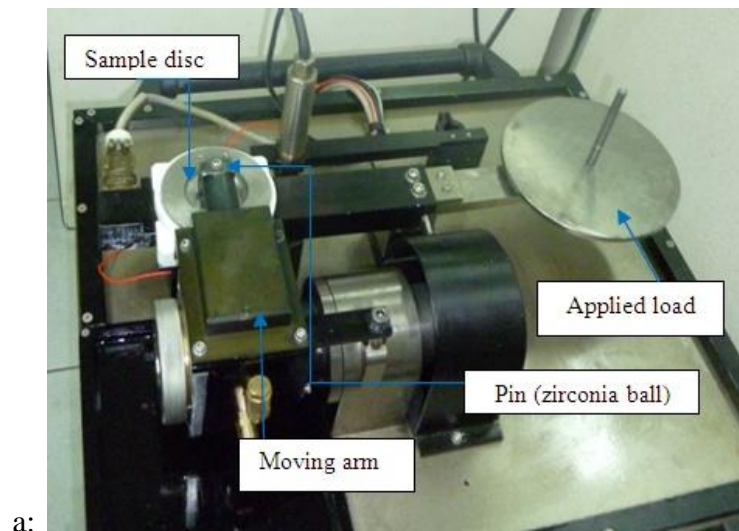


Figure 3.4. a: Pin-on-disc wearing machine; b: specimen fixed with epoxy inside suitable sample holder, and zirconia ball inside holder

wear was measured in a controlled air atmosphere. The temperature was set at 29°C and the relative humidity at 50%. The wear volume, V_w , was determined after a sliding distance, s , of 5 km. The wear volume, V_w , was determined by measuring the weight loss of the sample or by determination of the wear volume from the wear track depth as measured by interference profiling (ATOS micromap, Pfungstadt, Germany). Both measurements gave values of the same order of magnitude. The coefficient of friction is defined as the ratio between the measured friction force and the applied normal force. As with other mechanical properties, there are standard tests to measure wear resistance. The main method is described in ASTM G99, which uses a pin-on-disk apparatus.

CHAPTER 4 RESULTS AND DISCUSSION

4.1 Suspension analyses

4.1.1 Zeta potential

Zeta-potential behaviour of dilute suspension of alumina, yttria stabilised zirconia, magnesia and copper (II) oxide was investigated and Figure 4.1 presents the results for bare oxides without any surfactant and Figure 4.2.a and b present the results in the presence of Dolapix and Tiron respectively. The measured values for zeta-potential and IEP in this work is in good agreement with previous reports in literature, some works on Al_2O_3 , 3Y-TZP (Greenwood and Kendall, 1999) , copper(II) oxide (Guedes et al., 2009)and magnesia(Tari et al., 1997). There are also some different reports for zeta-potential as well for IEP which is explainable regards to different particle size of oxides, the electrolyte used as a background and its concentration(Franks and Meagher, 2003). Furthermore the reported value of zeta potential is affected significantly by the volume fraction of oxide (Delgado et al., 2005, Greenwood, 2003, Kosmulski, 2004). Reported Zeta potential value of concentrated and dilute suspensions shows different results with and without using background electrolytes. Zeta potential measurement with concentrated suspension are not affected by background solution as much as dilute suspension, it means in zeta measurement with dilute suspension it is important to use a suitable electrolyte to obtain high accuracy close to real value of particle charge.

According to zeta- potential value for bare oxides without any dispersant, the best pH area to make a stable suspension of Al_2O_3 , 3Y-TZP and CuO is in the pH out of their isoelectric point (IEP), $8.8 < \text{pH} < 5.4$, which the zeta charge is negative or positive for all of oxides, however the acidic region is limited because of the solubility of copper (II) oxide in pH range below 4. It is worth to note the practical pH is normally two unite away from IEP, in another word to have a stable suspension, the absolute value of zeta-potential should be more than 30 (Greenwood, 2003). In the case of addition of magnesia to the suspension of Al_2O_3 and 3Y-TZP the useful area to make a stable suspension will be limited to basic pH area because of the high solubility of magnesia in acidic pH which makes it impossible to use or to measure the electrophoretic mobility at pH values lower than pH 8. The IEP of bare magnesia is about pH 11 and above this point the zeta potential value is not enough big to make a stable suspension, in fact the opposite signs of surface charges on particles or an insufficient negative charge density on MgO particle surfaces will most likely lead to a hetero-coagulation phenomenon.

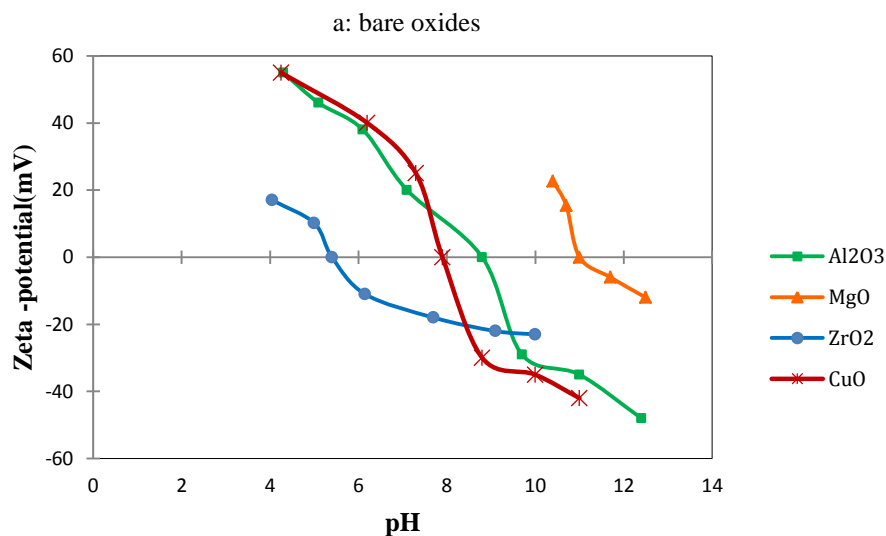


Figure 4.1 Zeta-potential of Al_2O_3 , 3Y-TZP, CuO and MgO as a function of pH without any surfactant.

In practical work at high volume fraction, even in pH above 11, it is difficult to obtain electrostatic stabilisation due to extensive double layer overlap, therefore it is necessary to adsorb polyelectrolytes onto the particles to stabilise the particles via steric or electrosteric mechanisms.

Addition of DolapixCE64 or Tiron as surfactant has a significant influence on zeta-potential value as well on the IEP. In the presence of 0.6 wt% Dolapix CE64 the IEP value for Al₂O₃, 3Y-TZP and CuO moves about two units to acidic direction and it is recorded at pH 6.4, 3.4 and 5.7 respectively. DolapixCE64 is a carbonic acid dispersant which it is ionized above pH 3.5 and is completely dissociated above pH8.5 (Prakash et al, 2007, Albano et al, 2002). This means that there could some weak interaction between the undissociated Dolapix CE64 and oxides surface through hydrogen bonding. Hence some reduction in the magnitude of zeta-potential is observed. In the pH range of 3.4 to 6.4 the dispersant starts ionizing and adsorption takes place due to electrostatic attraction between the positively charged surface and negatively charged functional groups of the dispersant. The charge reversal and increase in electronegativity in this pH range is based on concentration of the dispersant and amount of ionization. With increasing of pH the zeta-potential value of oxides gradually increase because of repulsion between negatively charged particles. Magnesia shows a negative value of zeta-potential in the presence of Dolapix and when the pH increase the absolute value for zeta charge is enough big to result a stable suspension. (Prakash et al,2007; Albano et al,2002).

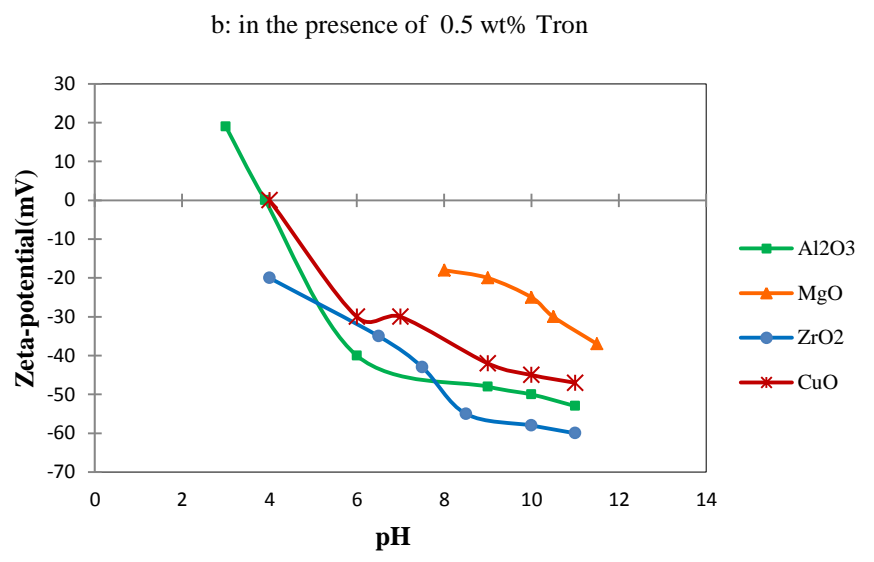
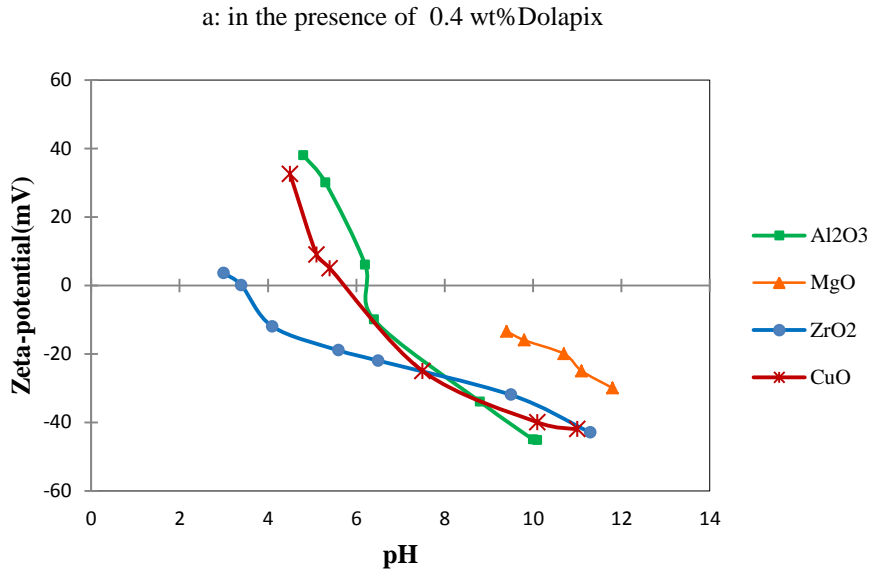


Figure 4.2. Zeta-potential of alumina, yttria stabilised zirconia, magnesia and copper (II) oxide in the *a*: presence of 0.4 wt % DolapixCE64 and *b*: presence of 0.5 wt% Tiron as a function of pH.

The presence of the dispersants enabled electrophoretic measurements further in the acidic direction, suggesting that the solubility of the MgO particles might have been diminished by formation of some type of complex on the surfaces independently of the dispersant used,

colloidal instability and almost complete dissolution of the MgO occurred before any isoelectric points could be detected.

Figure 4.2.b represents the changes in zeta-potential of named oxides in the affect of Tiron. The changes in the IEP value with 0.5 wt% Tiron moves another 2 unites for Al_2O_3 and CuO in acidic direction. The IEP value is not detected for zirconia but it is predicted to be in pH lower than 3.5 but the absolute value of zeta charge for this oxide is increased significantly. Tiron dissociates and adsorbs as negatively charged ion in alkaline region, however, in acidic region, it adsorbs mostly in a protonated form or as neutral molecule and it is because Tiron is essentially uncharged below pH 6, and fully ionized above pH 10. The adsorption of Tiron in the basic region occurs via specific interactions, i.e. an inner sphere complex is built between alcohol groups of the molecule and hydroxyl groups of alumina. A strong repulsive interaction between the oxide particles is created via negatively charged sulfonate, $-\text{SO}_3\text{Na}$, groups imparting stability to the suspension. This approach is well supported by authors who state that an electrolyte could be an efficient dispersant if functional group, which permit a strong adsorption, are different from those functionalities which form the surface charge. (Gulicovski et al., 2008)

4.1.2 Viscosity

The apparent viscosity of initially prepared single phase suspension of the Al_2O_3 and 3Y-TZP and their mixture with MgO and CuO was collected in Table 4.1. Suspension without any dispersant even in low concentration is not stable enough to test. The optimum amount of Dolapix CE64 and Tiron is according to previous works of other research about

alumina and stabilised zirconia and it used for this work and modified for mixture suspension of alumina, yttria stabilised zirconia, magnesia and copper (II) oxide.

Table 4.1 Apparent viscosity η_a for different suspensions.

Apparent Viscosity(mPa s)	The code number of suspensions from tables 3.3 and 3.4					
	(1)	(2)	(5)	(7)	(8)	(9)
Without dispersion In natural pH	Not flowing	Not stable	Not flowing	-	-	-
Dolapix CE64 0.4 wt%	10.4	7	16	10	7	20
Tiron 0.5wt%	8.2	5	9	8	4	14

4.1.3 pH

The natural pH value for different oxide changes with solid content and also different dispersants influence the pH value. Figure 4.3 represents the changes in pH value with increasing concentration of solid oxide in presence of Dolapix CE64 and Tiron.

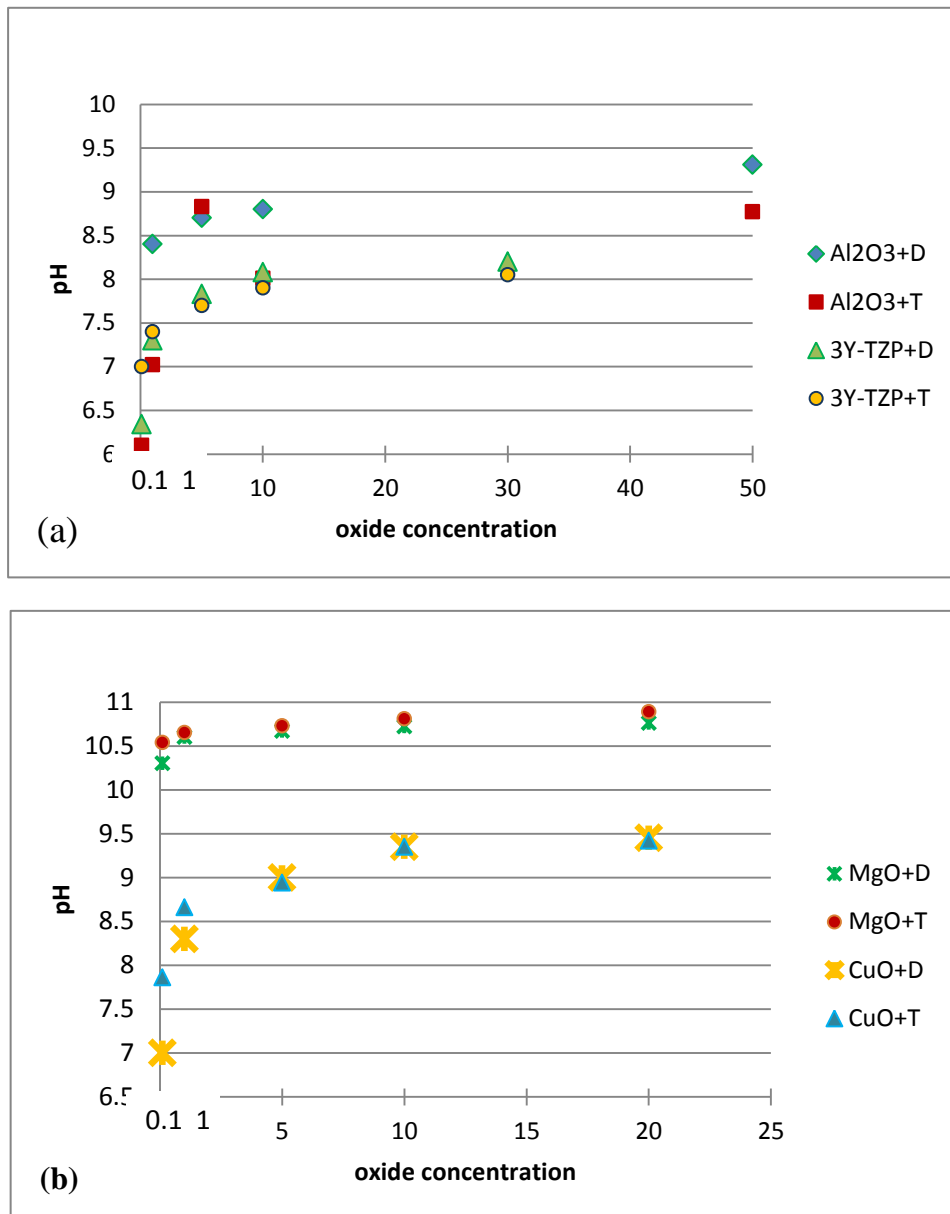


Figure 4.3 The pH change with increasing solid concentration in the presence of 0.4 wt% Dolapix and 0.5 wt% of Tiron (a): in alumina and yttria stabilised zirconia suspension; (b): in magnesia and copper (II) oxide suspension.

4.2 Sample Characterisation

4.2.1 Density

The bulk density of solid oxide powder used in this work is 3.988, 6.05, 3.58 and 6.31 g/cm³ for alumina, 3 mol yttria stabilized zirconia, magnesia and copper (II) oxide respectively. Therefore the theoretical density for ZTA composite with 85wt% Al₂O₃ and 15wt% 3Y-TZP (with volume fraction of 0.895 and 0.104 respectively) was measured 4.199 g/cm³. According to Table 4.2 the relative green density of samples prepared from 50wt% solid load suspension (samples: 1,6,7,8 and 9) are almost in same range (53-56), which is supported by the similarity in the shrinkage value for them. In the case of samples 2 and 5 prepared from 33.3 wt% and 60wt% solid load suspension the relative green density is 51 and 64 respectively and the shrinkage is 19.3 and 14.5 respectively, which means the relative green density and shrinkage strongly affected by the concentration of suspension. The samples prepared from concentrated suspension show relatively higher green density and lower percentage of shrinkage.

Table 4.2 The average density, shrinkage and porosity obtained for different compounds prepared using the suspensions with cod numbers taken from table 3.3 and 3.4.

Sample characterization (%)	1 Al ₂ O ₃	2 3Y-TZP	5 ZTA	6 ZTA	7 ZTA with MgO	8 ZTA with CuO	9 ZTA with MgO,CuO
Relative ρ_{green}	56	51	64	53.8	57	54.5	53.6
Relative ρ_{sintered}	99.26	99.64	98.93	98.87	99.62	98.45	99.31
Shrinkage	16	19.3	14.5	16.6	17	14.4	16
Closed Porosity	0.74	0.36	1.07	1.13	0.38	1.55	0.69

On the other hand the comparison of relative sintered density for samples 5 and 6 (both Al_2O_3 with 15 wt% 3Y-TZP prepared from 60 wt% and 50 wt% solid load suspension) demonstrates that the green density does not have affects the sintered density. The density of the composites decreases slightly with the increase of ZrO_2 , and it's signifying that the presence of zirconia particles prohibits the densification of alumina matrix. Although the solubility of ZrO_2 in Al_2O_3 is as low as 2000 ppm, the presence of Zr^{+4} solute can slow down the densification of alumina matrix (Tuan et al., 2002). The lowest sintered density is observed for ZTA sample with addition off 0.1 wt% copper (II) oxide which is 98.4 contrary to the results reported about the sintering aid beneficial influence of CuO on the sintering temperature and its function as sintering aid material (Ran et al., 2006, Ramesh and Gill, 2001), however it is considerable that the particle size of matrix and CuO have important role in sintering process, and sintering temperature or/and time shows increase in some case with addition of copper oxide to ceramic composites (Ran et al., 2007) and sometimes obtaining full density is not possible. The highest relative sintered density; 99.6 was recorded for sample 7 (ZTA with 0.05 wt% MgO). The density improvement of Al_2O_3 and 3Y-TZP ceramics as well as their composites (ZTA) by adding small amount of magnesia is explained as a result of development of liquid phase in the grain boundary which aid sintering process. Azhar et al (2011) studied on different magnesia particle size and they obtained the maximum density is by adding less than 1 wt% of 80nm magnesia particles to ZTA. Bernard Granger et al also worked on the addition of magnesia in alumina and reported higher density in compare with TiO_2 addition.(2007).

4.2.2 Microstructure and XRD

Scanning electron microscopy (SEM) images of sintered, polished and thermally etched samples of Al_2O_3 and 3Y-TZP are presented in Figure 4.4 and 4.6. The prepared

alumina ceramics sintered at 1500 °C indicates homogenous rough devoid of crack and typically enlarged grain of α -Al₂O₃ which is supported by the X-Ray diffraction pattern. In alumina compacts some secluded pores is observed which return to the porosity of samples measured around 0.8 % (the obtained relative density for alumina is 99.2%). The average grain size is 2±0.8 and it presages a high grain growth from the initial particle size of used powder (0.3-0.49 μ m).

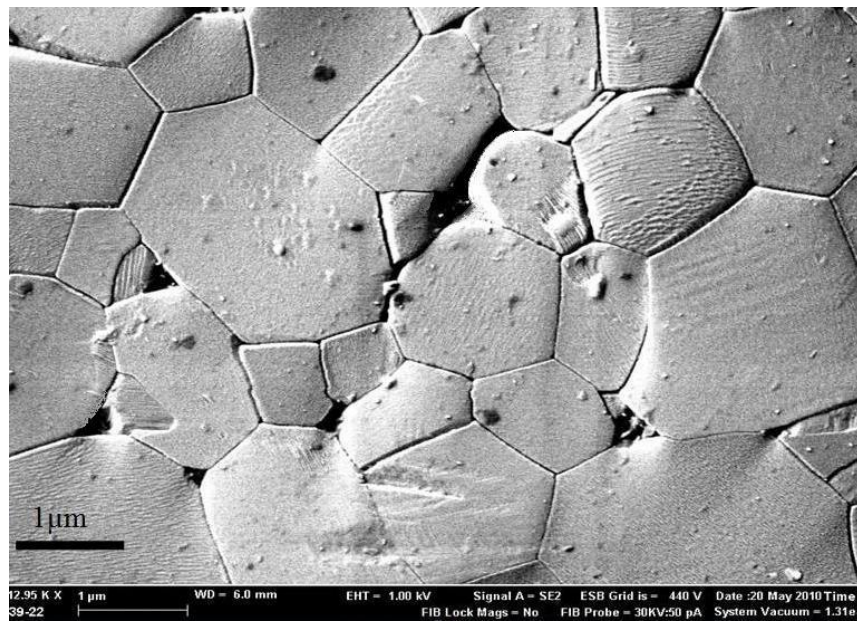


Figure 4.4 SEM image of polished and thermally etched alumina, the ceramic sintered at 1550 °C for 2 h in air.

The SEM image of 3Y-TZP shows very limit growth without any porosity in atomic scale, this characteristic is also reported in other researches(Nevarez-Rascon et al., 2009, Kim et al., 2004, Dillon and Harmer, 2007). In X-ray diffraction of as-received zirconia powder presented in Figure 4.6, the tetragonal and monoclinic phase both are observed, conversely the XRD pattern of 3Y-TZP samples (Figure 4.5) reveals that all zirconia crystallize in tetragonal phase and there is no observed pick for monoclinic.

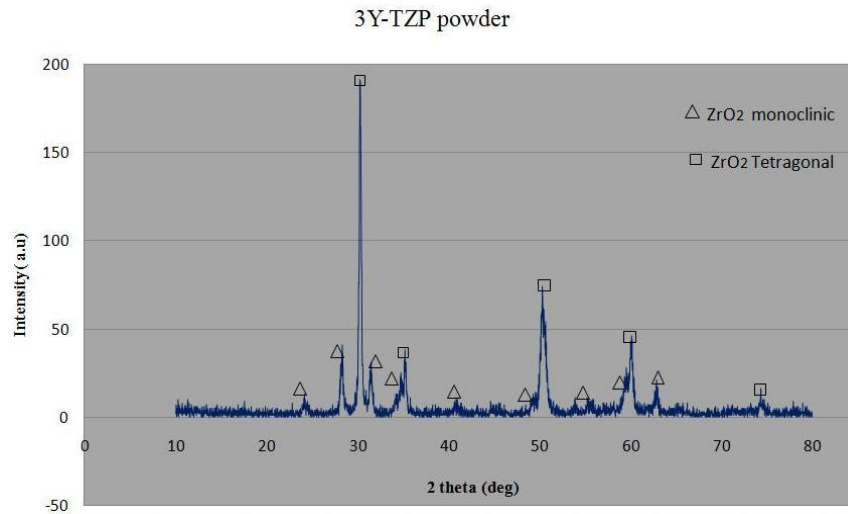


Figure 4.5. XRD of this-received 3Y-TZP powder.

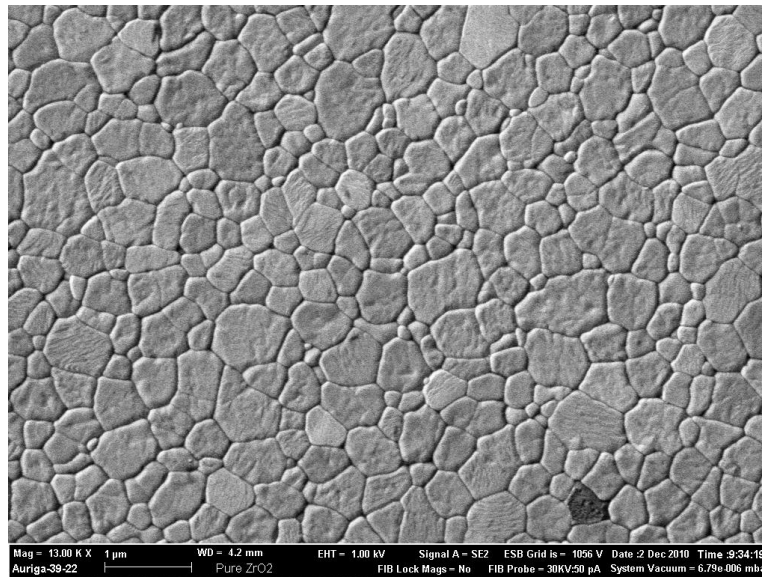


Figure 4.6 The SEM image of the polished and thermally etched 3Y-TZP. The ceramic sintered at 1550 °C for 2 h in air.

However, considering the $Y_2O_3-ZrO_2$ phase diagram, it is extremely possible to obtain cubic and tetragonal phases at sintering temperature of 1550 °C. According to this fact, the observed big grains in ZrO_2 seem to be cubic in nature, and this approval supported with the XRD pattern in Figure 4.7 corresponding to ZrO_2 stabilized with 5.3 wt% yttria in the reflection $2\theta = 74.67^\circ$.

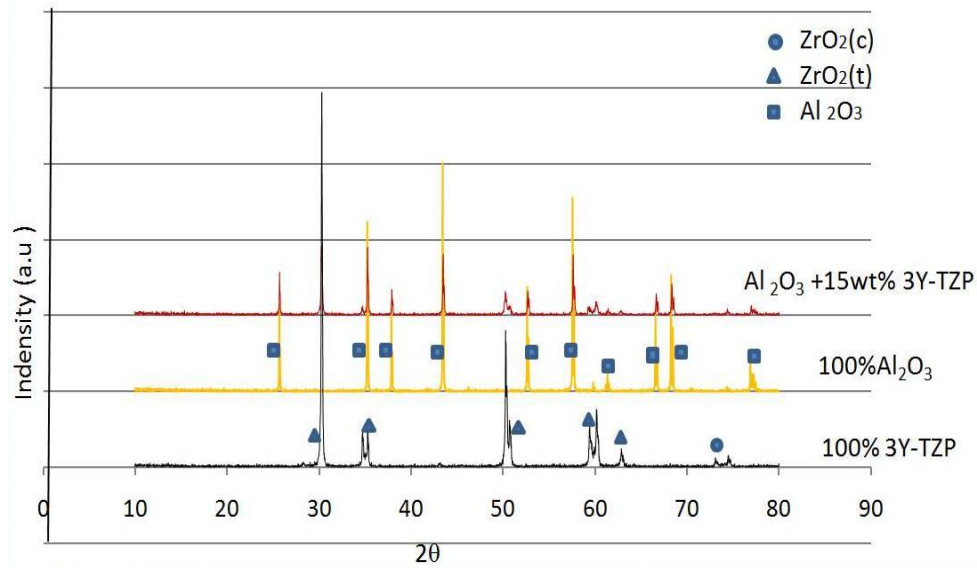


Figure 4.7 X- Ray diffraction pattern of sintered samples of Alumina, 3Y-TZP and ZTA.

SEM micrograph in figure 4.8 illustrates the homogeneous structure of ZTA composite which sintered in 1550 °C for 2h, the sample was prepared from suspension dispersed with 0.4 wt% Dolapix CE64 .The homogeneous distribution of 3Y-TZP particles in alumina matrix approve that no agglomeration or sedimentation took place during filtering process and presence of 3Y-TZP particles on the grain boundaries (bright area in Figure 4.9) suggests that they inhibit notably the alumina grain growth. The grain size of alumina particles in ZTA composite is 1.2 ± 0.5 which declare 40% decrease in compare with grain size of pure sintered alumina. This large reduction in particle size of alumina matrix is mostly observed in use of stabilized zirconia. Tuan, Chen et al (2002) investigated that the size of alumina grains in the t-Zirconia-containing composites is smaller than that in the m- zirconia-composites, indicating that the presence of a small amount of Y_2O_3 , the stabilizing agent for zirconia, can further prohibit the grain growth of alumina. Though the ionic charge of yttrium is the same as that of aluminum, the yttrium

ion is much larger than the aluminium ion (0.89 angstrom vs. 0.53 angstrom). Large yttrium ions tend to segregate at the grain boundaries of alumina, thus reducing elastic strain energy. Although the solubility of yttrium in alumina is extremely low (<10 ppm), large yttrium ions can block the diffusion of ions along grain boundaries, leading to reduced densification and grain growth rates.

Reciprocally the small change is observed in the particle size of 3Y-TZP which could be explained by inhibitor role of alumina particles. The average grain size of pure 3Y-TZP is 0.5 ± 0.3 and decreased to 0.3 ± 0.2 in ZTA composite. The obtained low grain growth for ZTA is supported by many others which they report the low grain growth rate for ZTA comparing with other nanocrystalline ceramics such as ZnO and Al_2O_3 (Mazaheri et al., 2009). From the XRD pattern of ZTA (Figure 4.7), it is observed that all 3Y-TZP particles crystallize in tetragonal form and there is no observed pick for monoclinic or cubic phase.

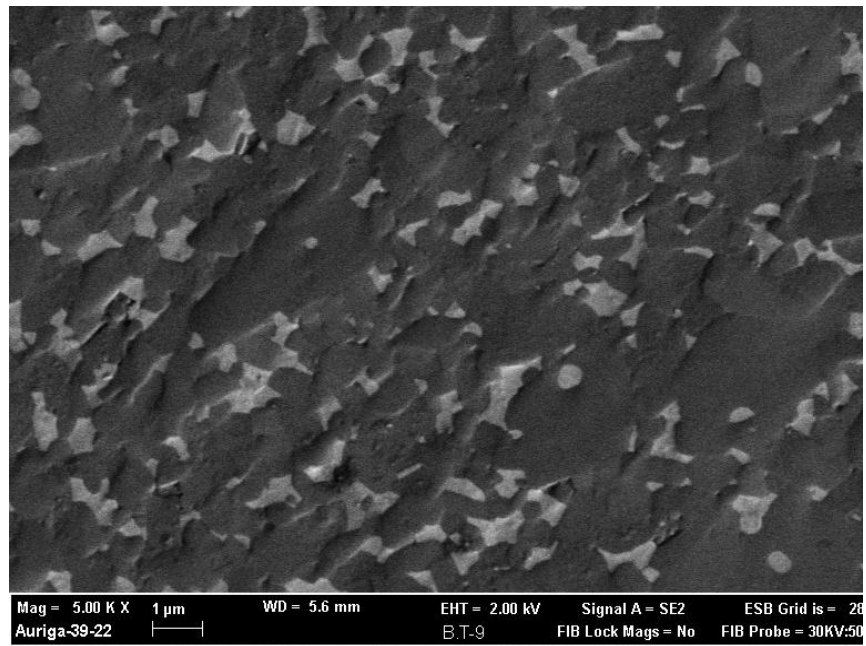


Figure 4.8 SEM micrograph of homogeneous ZTA (85wt% alumina and 15wt% 3Y-TZP), the bright area represents 3Y-TZP and dark area represents alumina particles.

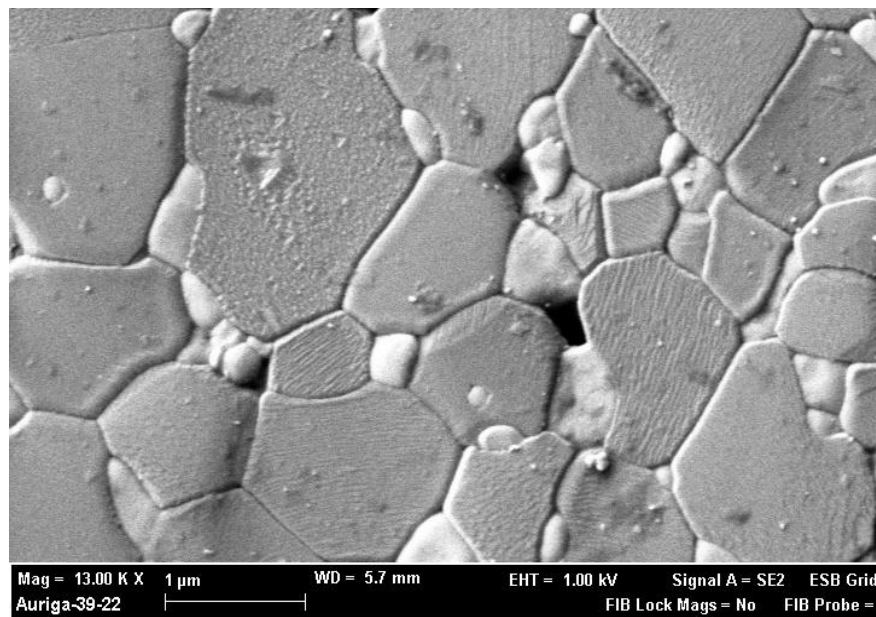


Figure 4.9. SEM image of ZTA, white color represents zirconia grain and gray color represents alumina particles.

Figure 4.10 shows a SEM image of ZTA composite with MgO addition .The measured particle size for alumina is 0.8 ± 0.4 which means the dispersion of small amount of MgO particles in ZTA acts as a powerful controller for alumina grain, despite there is

some large alumina particle as a consequence of abnormal grain growth, suggesting probably agglomeration in the starting suspension of ZTA+0.5 wt% MgO. More agglomeration in 3Y-TZP particles is observed in the case of using Dolapix CE64. Figure 4.11.A and B illustrate a comparative study between samples which prepared from dispersed suspension of Tiron and Dolapix CE64. The images were taken from different part of surface (three point of cross section: top, middle and bottom) .It is observed that using Tiron as dispersant results lower agglomeration rate of particles in the final composite.

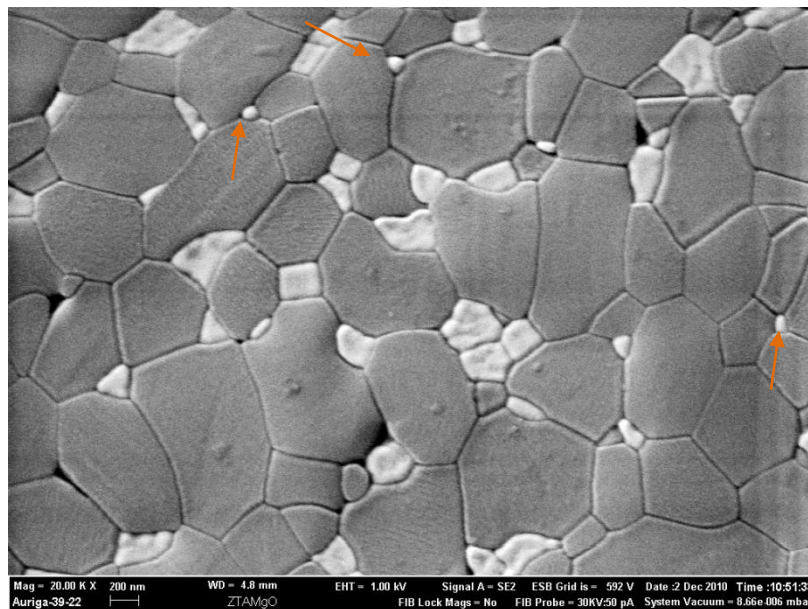


Figure 4.10 SEM of ZTA composite with 0.5wt% MgO, sintered, polished and thermally etched, the arrows point MgO particles

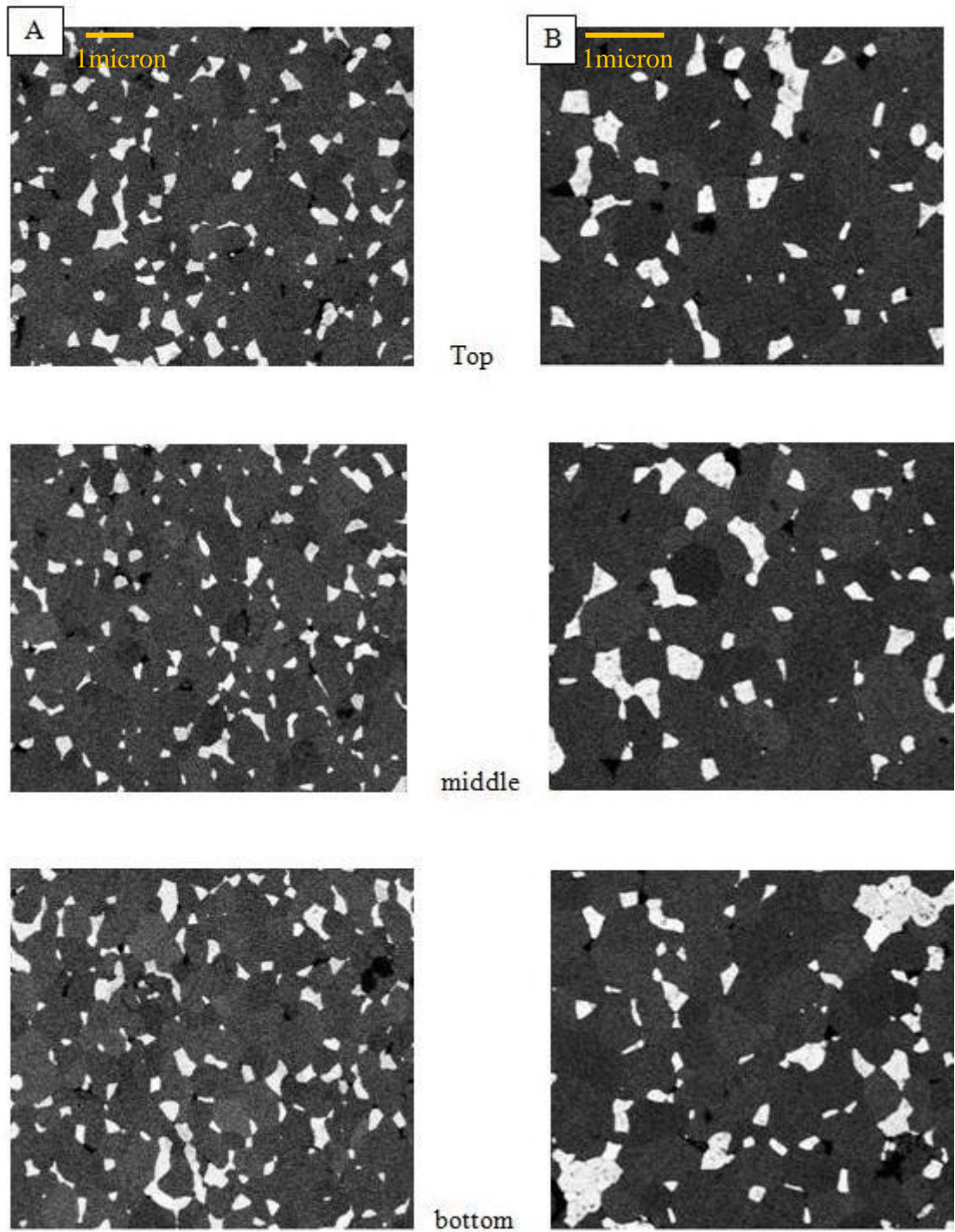


Figure 4.11 SEM micrograph taken from three different point at cross section of ZTA+ 0.5 wt% MgO samples prepared from A: suspension dispersed by Tiron; B: suspension dispersed by Dolapix

Figure 4.12 and 4.13 represent the SEM images of ZTA composite with addition of 1 wt% copper (II) oxide and ZTA composite with addition of both copper and magnesium

oxides, 0.1 wt% and 0.05 wt% respectively. As it is observed addition of CuO does not change the particle size of Al_2O_3 nor the particle size of 3Y-TZP. The composite of ZTA with MgO and CuO presents a homogeneous structure and it seems the MgO have the inhibition role for other alumina. The very small bright spots pointed by arrows (< 0.1 micron) represent the CuO particles.

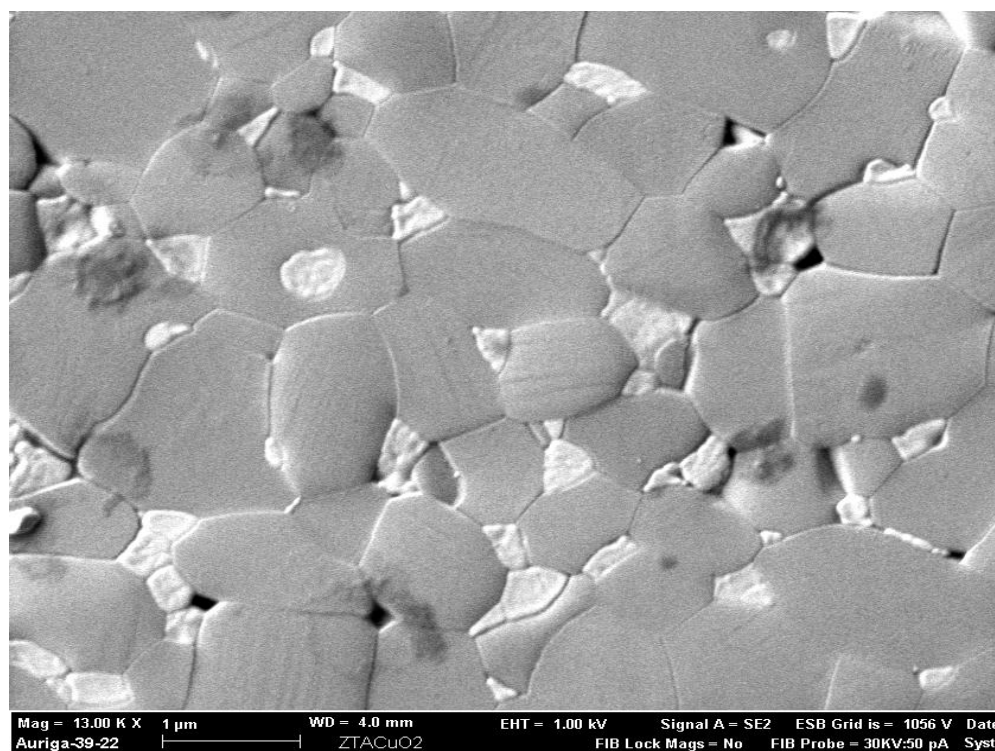


Figure 4.12 SEM of ZTA with 1 wt% CuO, the composite sintered at 1550 for 2h, polished and thermally etched.

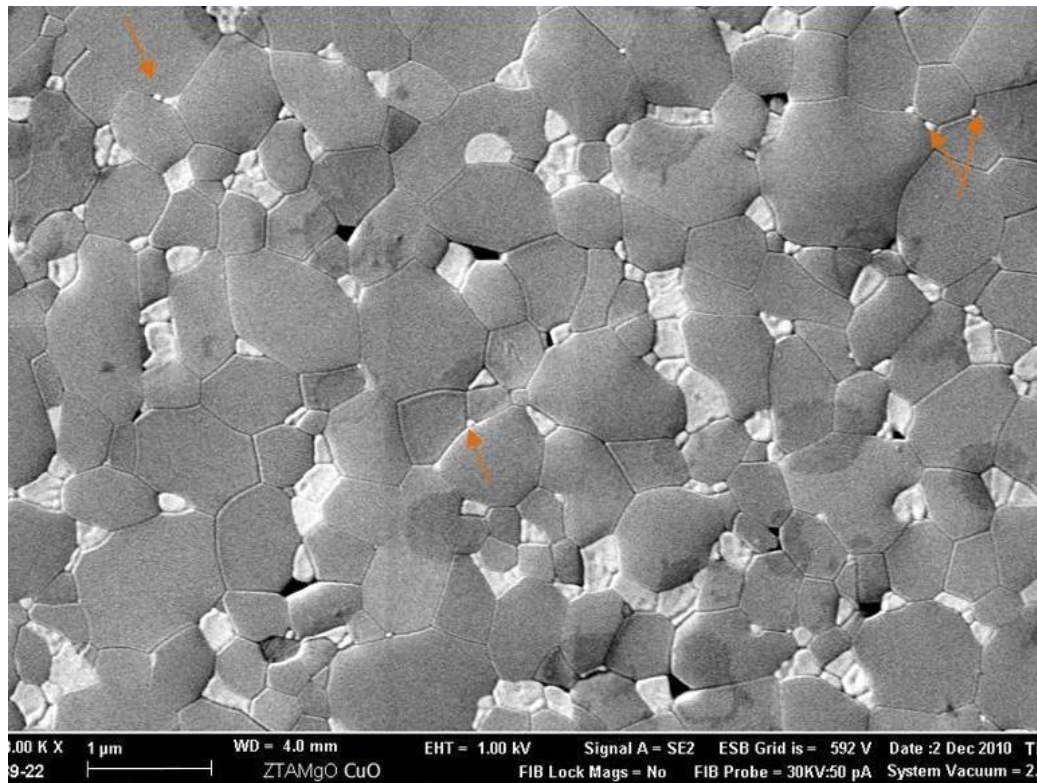


Figure 4.13 SEM image of ZTA with 0.05 wt% MgO and 0.1 wt% CuO; the gray area presents alumina, bright area presents zirconia and very small white spot pointed by arrows are the CuO and MgO particles

4.3 Mechanical properties

4.3.1 Hardness and fracture toughness

Figure 4.14 represents the hardness value of different compound measured by Vickers indentation method, with 10 kgf applied force, on the polished and thermally etched surface of the ceramics. The measured hardness before thermal etching and after polishing is also reported. The graph illustrates an extremely high value for hardness before thermal etching which could be explained by high preserved surface energy in the affect of polishing procedure. Furthermore the polishing procedure creates a high predisposition in tetragonal ZrO_2 particles for reforming to monoclinic, and this transformation consumes the energy of

indentation. The Vickers hardness for alumina is reported 19.7 GPa, referring to the high density of compound and originally high hardness of alumina ceramics, it is adequate to obtain high value of hardness for alumina. The Vickers hardness of 3Y-TZP is 15.5 GPa which is higher than 14 GPa of the conventional Y-TZP (Chevalier et al., 2004) and approximately close to the previous reports by Nevarez et al (2009) and De Aza et al (2002). The comparison of hardness value of two ZTA with high density (98.87 %) and low density (96.34%) which are 20.3 and 17.4 respectively. In compare with pure alumina ceramic the higher hardness value obtained for ZTA which it is explained as a result of the fine grain alumina matrix in ZTA (Lee and Speyer, 2002). The measured hardness for composite with 1 wt% CuO is 16.7 GPa and it is in the result of high volume of porosity and low density (98.45%), however the hardness of this compound is improved by adding magnesia and it is 19.3 GPa. The fine grain and the quantity of grain boundaries in this composite, it seems to be responsible for enhancing the hardness. In general the addition of MgO enhance the mechanical properties which is more significant when the finer particle of magnesia is added to ZTA .Mohamad Azhar et al (2011) reported that The result of the hardness values is closely related to the microstructure of ZTA. The maximum hardness which they report is 1740 Hv and it is obtained with the use of 80 nm MgO as additives. The compound with smaller Al₂O₃ grain size which resulted from the presence of MgO has got higher hardness. The role of MgO is to accelerate the sintering rate for Al₂O₃, thus hindering Al₂O₃ grains from growing.

We can conclude that Vickers hardness depends on the final porosity, its distribution and the grain size of the sintered substance. It is known that hardness of ceramic materials is usually affected by the intrinsic deformability of the ceramic and microstructural

parameters such as multiphases, grain size and orientation, porosity as well as boundary constitution (Tekeli, 2005) .

In the literature, the hardness and the fracture toughness values of ceramics are frequently reported as a function of the grain size. For example, hardness decreasing with temperature as a consequence of grain growth was reported by Echeberria et al. (2002).

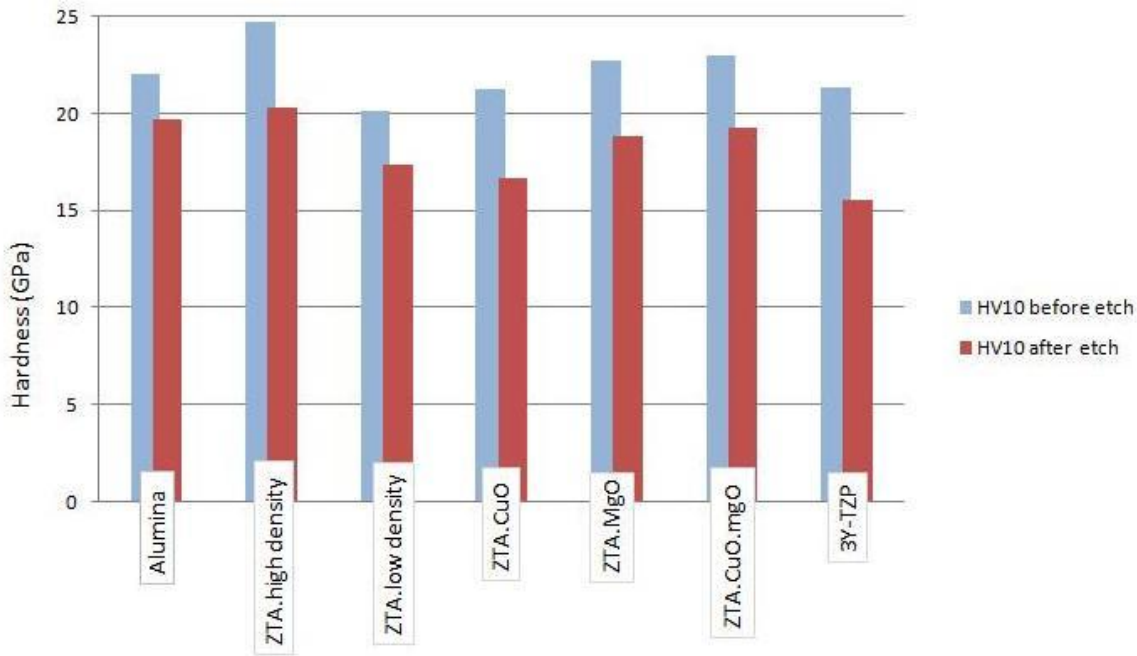


Figure 4.14 Vickers hardness value for different composites in 10 Kg load on the polished surface before and after thermal etching

Fracture toughness was measured by using indentation method (IM) and it is notable to consider that the value for fracture toughness reported by other authors are in wide range and extremely in high variation because of different used methods. For instance Casellas et al (1999) reported different values of K_{IC} by using distinct testing techniques. They reported that the measured K_{IC} by the IM and ISB methods are lesser than the evaluated values by

other methods. And also they explain that in the ceramics including zirconia the commonly used values of A and n (Anstis et al., 1981) do not give the actual fracture toughness as it has been recently shown for ceramics which undergo stress-induced phase transformation. In these ceramics, it seems that the value of A needs to be increased by 20% (A : 0.019) to account the additional crack driving force due to the indentation-induced transformation. However these parameters give acceptable value of fracture toughness for alumina (fine or coarse grained alumina).

Figure 4.15 presents fracture toughness of alumina, 3Y-TZP and their different compound. Two different value are reported (one obtained from general formula and other calculated by using Antis formula which improved for zirconia included ceramics by casellas)

As it is expected, the low K_{IC} value for alumina was improved with adding 15 wt% zirconia (K_{IC} for Al_2O_3 :1.72 and for ZTA: 4 $MPa \cdot m^{-1/2}$). This raise in fracture toughness for ZTA reveals that presence of tetragonal zirconia involves a considerable increase of K_{IC} . An important effect of the presence of tetragonal phase in the composite is that when the tetragonal (t) to monoclinic (m) phase transformation occurs, the resultant expansion will create compression zones that make it difficult the crack propagation from the defects of material. This beneficial effects of adding zirconia particles to alumina, was summarised by casellas et al. and several mechanisms have been pinpointed, First, transformation toughening, as induced from the stress-induced transformation experienced by tetragonal zirconia particles when interacting with an advancing

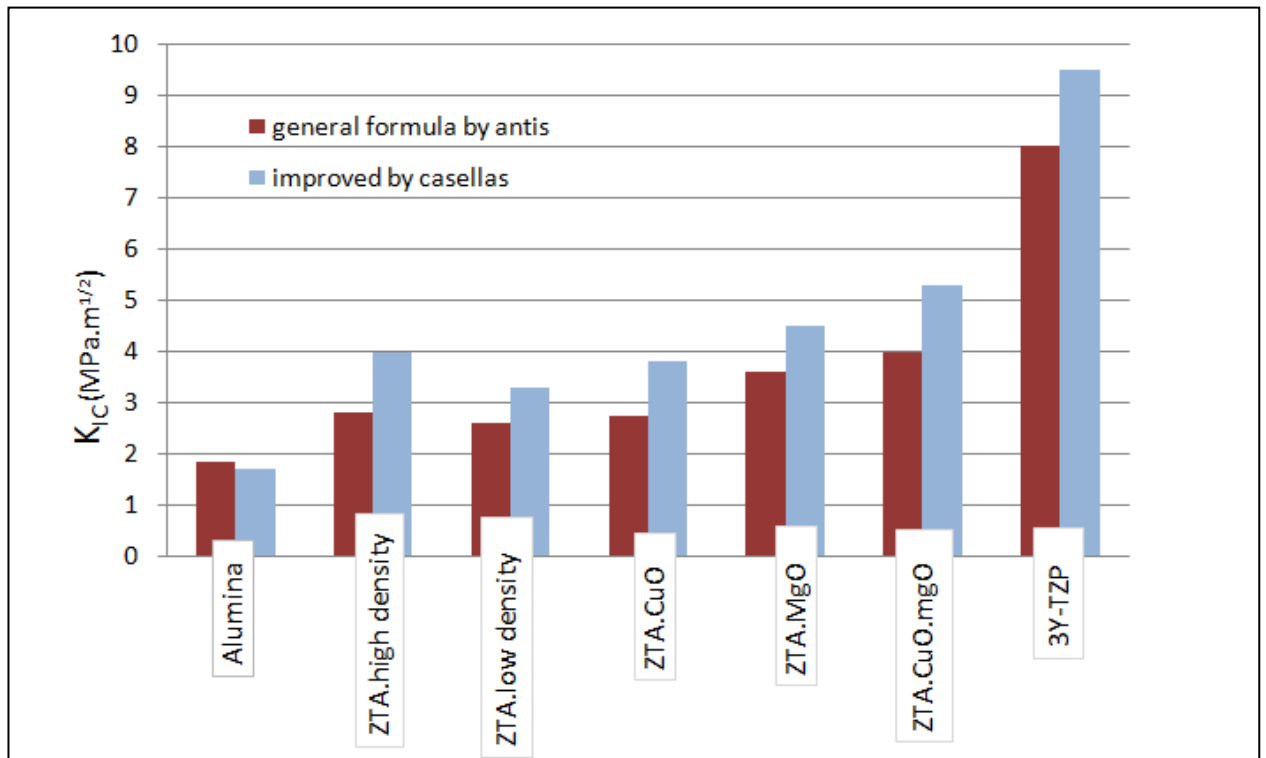


Figure 4.15 Fracture toughness (K_{IC}) value for different compound calculated with Antis-Casellas factors and general formula

crack, second, the effect of microcracks intrinsically related to such transformation, which then promote a toughening effect through the permanent dilatation and reduced modulus that they imply around the crack-tip. Third, the effect of internal stresses resulting from the differences in thermal expansion between the two phases, which set the alumina matrix under compressive residual stresses. It is worth to note that the toughness of ZTA composite could reach to the higher amount if there is an initially amount of monoclinic zirconia ($m\text{-ZrO}_2$) which is possible by using ($m\text{-ZrO}_2$) or mixture of $m\text{-ZrO}_2$ and $t\text{-ZrO}_2$ (Tuan et al., 2002). In this work the XRD pattern of sintered samples doesn't show any $m\text{-ZrO}_2$, however it is predicted that the amount of $m\text{-ZrO}_2$ on the fractured surface reach to 10wt%. The more increase in the K_{IC} values observed for ZTA composite with MgO which is because of finer grain and high density of these composite.

4.3.2 Wearing

The coefficient of friction as an important factor in understanding of tribological behaviour is collected for all compound for sliding distance of 4000m against the zirconia ball. As it is well known the coefficient of friction of alumina-zirconia ceramics against zirconia ball generally is high in compare with its value when is measured against alumina ball (Suh et al., 2008, Kerkwijk et al., 1999). It is prominent to note for comparing the result of wearing test it is important to consider the velocity, humidity and normal load which is applied.

As it is observed from Figure 4.16 the highest value was measured for 3Y.TZP (0.68 to 0.79) and this value is lower than the reported coefficient of friction in literature (Kerkwijk et al., 2004) The measured value for alumina is the lowest which in the starting is 0.41 and in the end of testing distance increases to 0.57. Coefficient of friction value for ZTA is approximately average of this value for Al_2O_3 and 3Y-TZP. Surprisingly the coefficient of friction for composite with copper (II) oxide starts from high point around 0.71 however with distance decrease to 0.64. Adding 1wt% copper (II) oxide to alumina has been reported as a best addition amount for decreasing coefficient of friction to 0.4 against alumina ball and against zirconia ball it decrease to 0.52. in the same velocity (0.1 m/s)(Pasaribu et al., 2005).The coefficient of friction for ZTA composite with MgO and with MgO-CuO does not show any improvement.

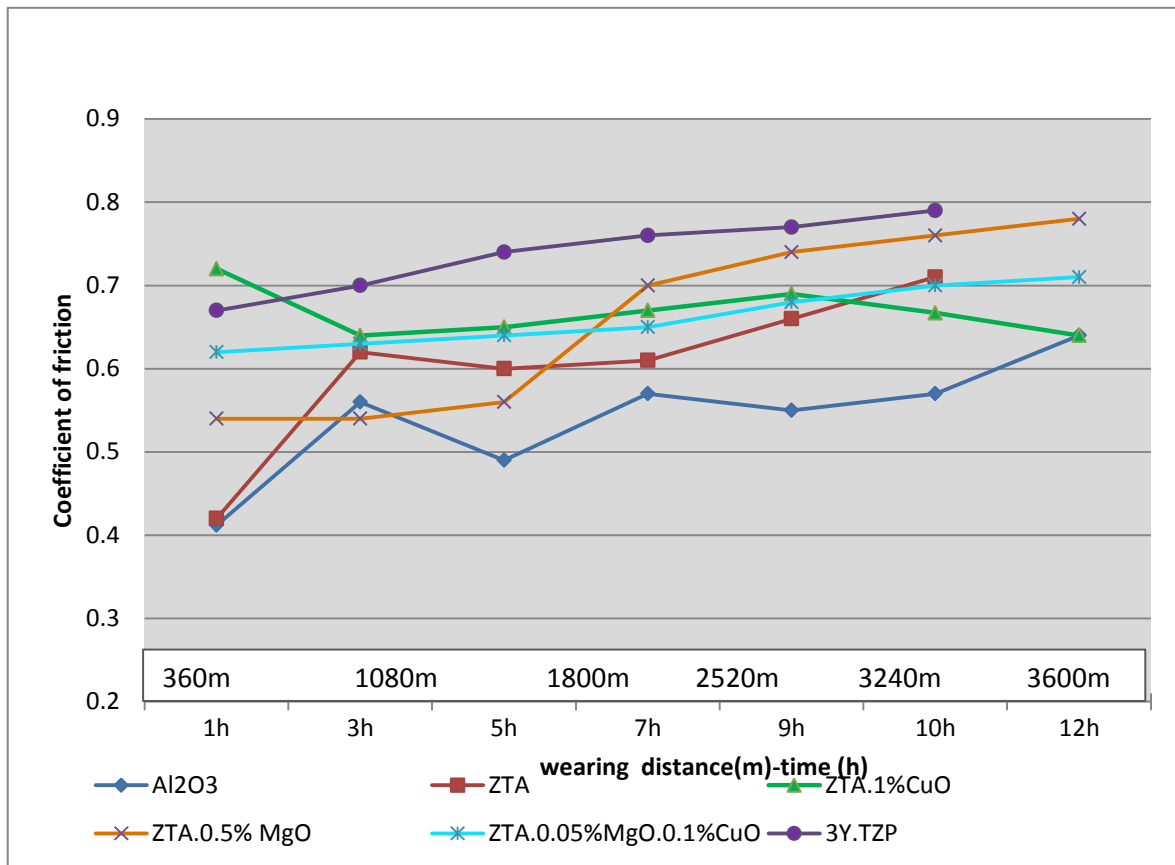


Figure 4.16 Coefficient of friction changes with sliding distance (m) up to 3600m for sintered, polished and thermally etched samples.

Figure 4.17 represents the wearing volume (mm^3) during a period of time for different compounds. The total wearing for 3Y-TZP and for MgO-doped ZTA is quite high, however the wear-time curve for them follow totally different pattern. The high wearing volume and high

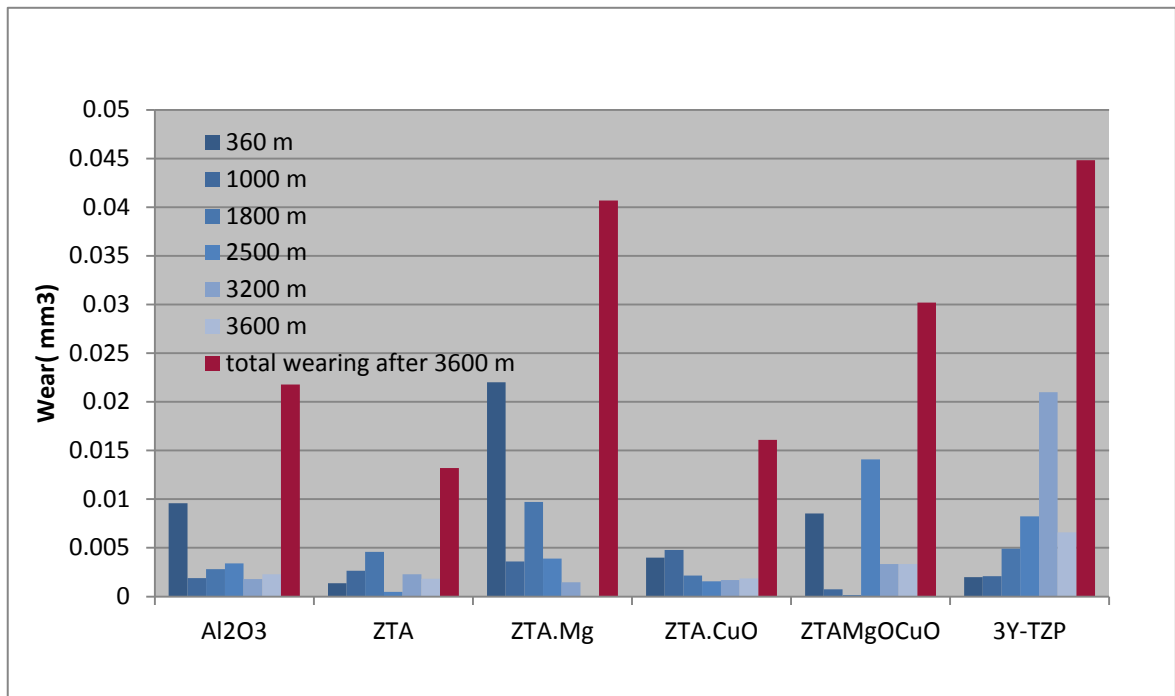


Figure 4.17 The worn volume (mm^3) for different compounds as a function of the sliding distance at a sliding speed of 0.1 m/s with zirconia ball.

wearing rate of zirconia compound against zirconia ball has been reported by Min.Soo.Suh et.al (2007). ZTA composite and CuO-doped ZTA show the high wearing resistant and the total wear after 3600 m is low in compare with other samples.

CHAPTER 5 CONCLUSION AND RECOMMENDATION

5.1 Conclusion

This study describes an experimental method for the producing of ZTA composite which zirconia in the form of yttria stabilised particles (3Y-TZP) is dispersed homogeneously in an alumina (Al_2O_3) matrix. The study presents the elevated mechanical properties for magnesia or/and copper (II) oxide doped ZTA. Achieving to a good dispersion of 3Y-TZP as well as magnesium and copper (II) oxides is possible by employing surfactant in the suitable pH region. Two kinds of surfactant were investigated and comparison study is presented. According to the experimental results, the following conclusion can be drawn:

1. The studies on the Zeta-potential and viscosity of different slurries confirmed that in the basic pH region (above 9) the suspension of alumina, zirconia, magnesia and copper (II) oxides in the presence of Dolapix and Tiron are stable.
2. The SEM images of cross section of the composites confirm that in the presence of both surfactants the dispersion of zirconia particles in alumina matrix is uniform and no agglomeration take place in the filtration step. However magnesia-doped composite shows agglomeration of zirconia particles in the presence of Dolapix, but full homogenous structure observes with Tiron.
3. Again, from the SEM images, it can be concluded that the grain size of alumina decrease in the presence of zirconia particles. Despite microstructure of ZTA composite contains more pores, which they appear in the grain boundary and form a

low density ceramic. The addition of magnesia to ZTA composites (0.5 wt %) enhances the microstructure properties of composite and ceramic with high density and finer grain size is obtained.

4. Comparing the green and sintered density of ZTA composites suggests that the density of green compact does not affect the density of compact after sintering. In fact it is possible to obtain high density for a compound with a low green density however the shrinkage will be increase in this case.
5. Reinforcement of alumina by stabilised zirconia enhances both hardness and fracture toughness of ZTA composites (20.3 GP, 4 MPa.m^{-1/2})
6. The fracture toughness for CuO-MgO-doped ZTA shows 32.5% increase in compare with un-doped ZTA but the hardness value shows just 4.9 % decrease.
7. The coefficient of friction for CuO-doped ceramic decrease with distance, however the coefficient of friction for doped-ZTA is in the same range of non-doped ZTA and also the wearing resistance of doped ZTA doesn't improve in comparison with un doped ZTA.

5.2 Recommendation

This study focused on the producing and investigating different mechanical properties of ZTA with 85 wt% Al₂O₃ and 15 wt% ZrO₂. Compleitive study on the ZTA composites with different fraction of alumina and zirconia could be useful to learn more about the influence of magnesia (MgO) on the particle size and other properties of ZTA structure.

Moreover in this study stabilised zirconia with submicron grain size was used, despite using mixture of unstabilised and stabilised zirconia could effectively strengthen the

toughening properties of ZTA composites , then the study on the possibility of obtaining homogeneous composite structure using stabilised and unstabilised zirconia is recommended .

The using nano particle magnesia more than 0.5 wt% makes difficulties for the flowing properties of aqueous suspension of alumina and zirconia and leads to an agglomerated suspension. Therefore the study on using submicron magnesia is recommended to develop the application range for magnesia.

REFERENCES

- Aminzare, M., F. Golestani-fard, O. Guillon, M. Mazaheri & H. R. Rezaie (2010) Sintering behavior of an ultrafine alumina powder shaped by pressure filtration and dry pressing. *Materials Science and Engineering: A*, 527, 3807-3812.
- Aminzare, M., M. Mazaheri, F. Golestani-fard, H. R. Rezaie & R. Ajeian (2011) Sintering behavior of nano alumina powder shaped by pressure filtration. *Ceramics International*, 37, 9-14.
- Anstis, G., P. Chantikul, B. R. Lawn & D. Marshall (1981) A critical evaluation of indentation techniques for measuring fracture toughness: I, direct crack measurements. *Journal of the American Ceramic Society*, 64, 533-538.
- Azhar, A. Z. A., H. Mohamad, M. M. Ratnam & Z. A. Ahmad (2011) Effect of MgO particle size on the microstructure, mechanical properties and wear performance of ZTA-MgO ceramic cutting inserts. *International Journal of Refractory Metals and Hard Materials*, 29, 456-461.
- Bennison, S. J. & M. P. Harmer (1983) Effect of MgO Solute on the Kinetics of Grain Growth in Al₂O₃. *Journal of the American Ceramic Society*, 66, C 90-C 92.
- Bernard-Granger, G. & C. Guizard (2007) Influence of MgO or TiO₂ doping on the sintering path and on the optical properties of a submicronic alumina material. *Scripta Materialia*, 56, 983-986.
- Bormans, P. 2004. *Ceramics are more than clay alone*. Cambridge International Science Publishing.
- Briscoe, B. J., A. U. Khan & P. F. Luckham (1998) Stabilising zirconia aqueous suspensions using commercial polyvalent electrolyte solutions. *Journal of the European Ceramic Society*, 18, 2169-2173.
- Cardarelli, F. 2008. *Ceramics, Refractories, and Glasses*. In *Materials Handbook*, 593-689. Springer London.
- Carter, C. B. & M. G. Norton. 2007. *Ceramic materials: science and engineering*. Springer Verlag.
- Casellas, D., I. R. fols, L. Llanes & M. Anglada (1999) Fracture toughness of zirconia-alumina composites. *International Journal of Refractory Metals and Hard Materials*, 17, 11-20.
- Chevalier, J. (2006) What future for zirconia as a biomaterial? *Biomaterials*, 27, 535-543.
- Chevalier, J. J., S. Deville, E. Munch, R. Jullian & F. Lair (2004) Critical effect of cubic phase on aging in 3 mol% yttria-stabilized zirconia ceramics for hip replacement prosthesis. *Biomaterials*, 25, 5539-5545.
- De Aza, A. H., J. Chevalier, G. Fantozzi, M. Schehl & R. Torrecillas (2002) Crack growth resistance of alumina, zirconia and zirconia toughened alumina ceramics for joint prostheses. *Biomaterials*, 23, 937-945.
- Delgado, A., F. Gonzalez-Caballero, R. Hunter, L. Koopal & J. Lyklema (2005) Measurement and interpretation of electrokinetic phenomena. *Pure Appl. Chem*, 77, 1753-1805.
- Delgado, A. V., F. González-Caballero, R. J. Hunter, L. K. Koopal & J. Lyklema (2007) Measurement and interpretation of electrokinetic phenomena. *Journal of Colloid and Interface Science*, 309, 194-224.
- Dey, A. K. & K. Biswas (2009) Dry sliding wear of zirconia-toughened alumina with different metal oxide additives. *Ceramics International*, 35, 997-1002.
- Dillon, S. J. & M. P. Harmer (2007) Multiple grain boundary transitions in ceramics: A case study of alumina. *Acta Materialia*, 55, 5247-5254.
- Echeberria, J., J. Tarazona, J. He, T. Butler & F. Castro (2002) Sinter-HIP of [alpha]-alumina powders with sub-micron grain sizes. *Journal of the European Ceramic Society*, 22, 1801-1809.

- Franks, G. V. & L. Meagher (2003) The isoelectric points of sapphire crystals and alpha-alumina powder* 1. *Colloids and Surfaces A: Physicochemical and Engineering Aspects*, 214, 99-110.
- Greenwood, R. (2003) Review of the measurement of zeta potentials in concentrated aqueous suspensions using electroacoustics. *Advances in Colloid and Interface Science*, 106, 55-81.
- Greenwood, R. & K. Kendall (1999) Selection of suitable dispersants for aqueous suspensions of zirconia and titania powders using acoustophoresis. *Journal of the European Ceramic Society*, 19, 479-488.
- Guedes, M., J. M. F. Ferreira & A. C. Ferro (2009) A study on the aqueous dispersion mechanism of CuO powders using Tiron. *Journal of Colloid and Interface Science*, 330, 119-124.
- Gulicovski, J. J., L. S. Cerovic & S. K. Milonjic (2008) Stability of alumina suspensions in the presence of Tiron. *Ceramics International*, 34, 23-26.
- Harper, C. A. 2001. *Handbook of ceramics, glasses, and diamonds*. McGraw-Hill Professional.
- Kerkwijk, B., M. García, W. E. van Zyl, L. Winnubst, E. J. Mulder, D. J. Schipper & H. Verweij (2004) Friction behaviour of solid oxide lubricants as second phase in [alpha]-Al₂O₃ and stabilised ZrO₂ composites. *Wear*, 256, 182-189.
- Kerkwijk, B., A. J. A. Winnubst, H. Verweij, E. J. Mulder, H. S. C. Metselaar & D. J. Schipper (1999) Tribological properties of nanoscale alumina-zirconia composites. *Wear*, 225-229, 1293-1302.
- Kim, M. J., Y. K. Cho & D. Y. Yoon (2004) Kinked grain boundaries in alumina doped with Y₂O₃. *Journal of the American Ceramic Society*, 87, 717-719.
- Kosmulski, M. (2004) pH-dependent surface charging and points of zero charge II. Update. *Journal of Colloid and Interface Science*, 275, 214-224.
- KUNEŠ, K., J. HAVRDA, K. HRONÍKOVÁ, E. GREGOROVÁ & W. PABST (2000) Stabilization of bioceramic suspensions prepared from alumina-containing zirconia powders. *Ceramics-Silikáty*, 44, 1-8.
- Lance, D., F. Valdivieso & P. Goeriot (2004) Correlation between densification rate and microstructural evolution for pure alpha alumina. *Journal of the European Ceramic Society*, 24, 2749-2761.
- Lawn, B. & R. Wilshaw (1975) Indentation fracture: principles and applications. *Journal of materials science*, 10, 1049-1081.
- Lee, H. & R. F. Speyer (2002) Hardness and Fracture Toughness of Pressureless Sintered Boron Carbide (B₄C). *Journal of the American Ceramic Society*, 85, 1291-1293.
- Lorenzo-Martin, C., O. O. Ajayi, R. A. Erck & J. L. Routbort (2009) Tribo-mechanical etching of structural ceramic materials during lubricated severe sliding contact. *Wear*, 267, 608-613.
- Maarten Biesheuvel, P. (2000) Particle segregation during pressure filtration for cast formation. *Chemical Engineering Science*, 55, 2595-2606.
- Maarten Biesheuvel, P. & H. Verweij (2000) Influence of suspension concentration on cast formation time in pressure filtration. *Journal of the European Ceramic Society*, 20, 835-842.
- Mazaheri, M., A. Simchi, M. Dourandish & F. Golestani-Fard (2009) Master sintering curves of a nanoscale 3Y-TZP powder compacts. *Ceramics International*, 35, 547-554.
- Meza, J. & C. Chaves (2003) Estimación de la tenacidad a la fractura mediante el método de indentación. *Dyna*, 139, 53-59.
- Michálková, M., K. Ghillányová & D. Galusek (2010) The influence of solid loading in suspensions of a submicrometric alumina powder on green and sintered pressure filtrated samples. *Ceramics International*, 36, 385-390.
- Mishra, R. S. & A. K. Mukherjee (2001) Processing of high hardness-high toughness alumina matrix nanocomposites. *Materials Science and Engineering A*, 301, 97-101.
- Moghadas, S., A. Maghsoudipour, M. Alizadeh & T. Ebadzadeh (2011) Investigation on rheological behavior of 8 mol% yttria stabilized zirconia (8YSZ) powder using Tiron. *Ceramics International*.

- Nevarez-Rascon, A., A. Aguilar-Elguezabal, E. Orrantia & M. Bocanegra-Bernal (2009) On the wide range of mechanical properties of ZTA and ATZ based dental ceramic composites by varying the Al₂O₃ and ZrO₂ content. *International Journal of Refractory Metals and Hard Materials*, 27, 962-970.
- Pasaribu, H. R., K. M. Reuver, D. J. Schipper, S. Ran, K. W. Wiratha, A. J. A. Winnubst & D. H. A. Blank (2005) Environmental effects on friction and wear of dry sliding zirconia and alumina ceramics doped with copper oxide. *International Journal of Refractory Metals and Hard Materials*, 23, 386-390.
- Raether, F. & P. Schulze Horn (2009) Investigation of sintering mechanisms of alumina using kinetic field and master sintering diagrams. *Journal of the European Ceramic Society*, 29, 2225-2234.
- Rafferty, A., A. M. Alsebaie, A. G. Olabi & T. Prescott (2009) Properties of zirconia-toughened-alumina prepared via powder processing and colloidal processing routes. *Journal of Colloid and Interface Science*, 329, 310-315.
- Ramesh, S. & C. Gill (2001) Environmental degradation of CuO-doped Y-TZP ceramics. *Ceramics International*, 27, 705-711.
- Ran, S., L. Winnubst, D. H. A. Blank, H. R. Pasaribu, J. W. Sloetjes & D. J. Schipper (2007) Effect of Microstructure on the Tribological and Mechanical Properties of CuO Doped 3Y TZP Ceramics. *Journal of the American Ceramic Society*, 90, 2747-2752.
- Ran, S., L. Winnubst, W. Wiratha & D. H. A. Blank (2006) Sintering Behavior of 0.8 mol% CuO Doped 3Y TZP Ceramics. *Journal of the American Ceramic Society*, 89, 151-155.
- Reed, J. S. 1995. *Principles of ceramics processing*. Wiley.
- Riedel, R. 2000. *Handbook of ceramic hard materials*. Wiley-Vch.
- Schwartz, M. M. (1991) *Handbook of structural ceramics*.
- Suh, M. S., Y. H. Chae & S. S. Kim (2008) Friction and wear behavior of structural ceramics sliding against zirconia. *Wear*, 264, 800-806.
- Szutkowska, M. (2004) Fracture resistance behavior of alumina-zirconia composites. *Journal of Materials Processing Technology*, 153, 868-874.
- Tari, G., J. M. F. Ferreira & O. Lyckfeldt (1997) Influence of magnesia on colloidal processing of alumina. *Journal of the European Ceramic Society*, 17, 1341-1350.
- Tekeli, S. (2005) Fracture toughness (K_{IC}), hardness, sintering and grain growth behaviour of 8YSCZ/Al₂O₃ composites produced by colloidal processing. *Journal of Alloys and Compounds*, 391, 217-224.
- Tuan, W., R. Chen, T. Wang, C. Cheng & P. Kuo (2002) Mechanical properties of Al₂O₃/ZrO₂ composites. *Journal of the European Ceramic Society*, 22, 2827-2833.
- Wang, J. & R. Stevens (1989) Zirconia-toughened alumina (ZTA) ceramics. *Journal of materials science*, 24, 3421-3440.
- Wang, Y. & S. M. Hsu (1996) Wear and wear transition modeling of ceramics. *Wear*, 195, 35-46.
- Wang, Y., F. Worzala & A. Lefkow (1993) Friction and wear properties of partially stabilized zirconia with solid lubricant. *Wear*, 167, 23-31.

APPENDIX A: ZETA POTENTIAL MEASUREMENT

Zeta potential measurement for :

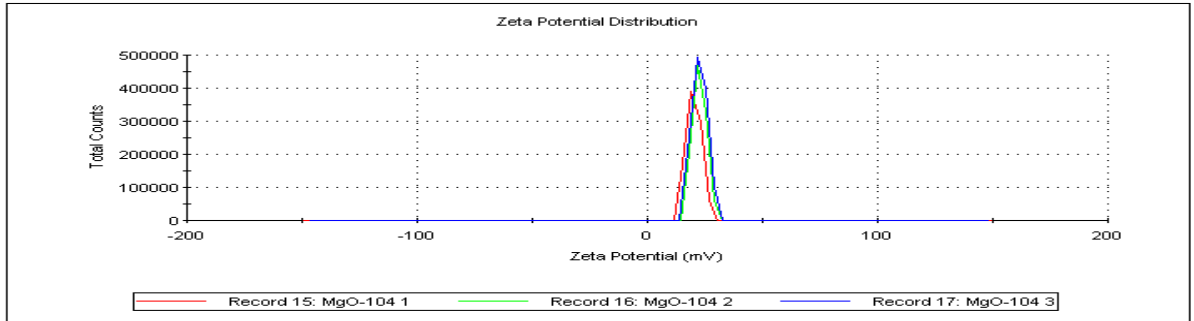
- Magnesia
- Copper (II) oxide
- Alumina
- Zirconia (3Y-TZP)

Sample Name: MgO-104 3
SOP Name: MgO104.sop
File Name: testing.dts
Record Number: 17
Date and Time: Tuesday, October 19, 2010 3:23:13 PM
Dispersant Name: Water
Dispersant RI: 1.330
Viscosity (cP): 0.8870
Dispersant Dielectric Constant: 78.5

Temperature (°C): 25.1
Count Rate (kcps): 136.1
Cell Description: Clear disposable zeta cell
Zeta Runs: 12
Measurement Position (mm): 2.00
Attenuator: 7

	Mean (mV)	Area (%)	Width (mV)
Zeta Potential (mV): 22.7	Peak 1: 22.7	100.0	3.21
Zeta Deviation (mV): 3.21	Peak 2: 0.00	0.0	0.00
Conductivity (mS/cm): 1.30	Peak 3: 0.00	0.0	0.00

Result quality : Good

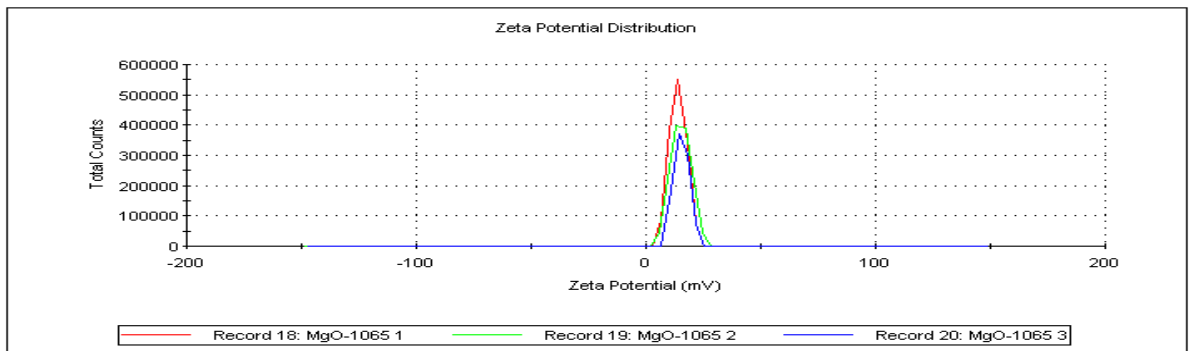


Sample Name: MgO-1065 3
SOP Name: MgO1065.sop
File Name: testing.dts
Record Number: 20
Date and Time: Tuesday, October 19, 2010 3:30:03 PM
Dispersant Name: Water
Dispersant RI: 1.330
Viscosity (cP): 0.8881
Dispersant Dielectric Constant: 78.5

Temperature (°C): 25.1
Count Rate (kcps): 66.6
Cell Description: Clear disposable zeta cell
Zeta Runs: 12
Measurement Position (mm): 2.00
Attenuator: 5

	Mean (mV)	Area (%)	Width (mV)
Zeta Potential (mV): 15.4	Peak 1: 15.4	100.0	3.19
Zeta Deviation (mV): 3.19	Peak 2: 0.00	0.0	0.00
Conductivity (mS/cm): 0.182	Peak 3: 0.00	0.0	0.00

Result quality : Good

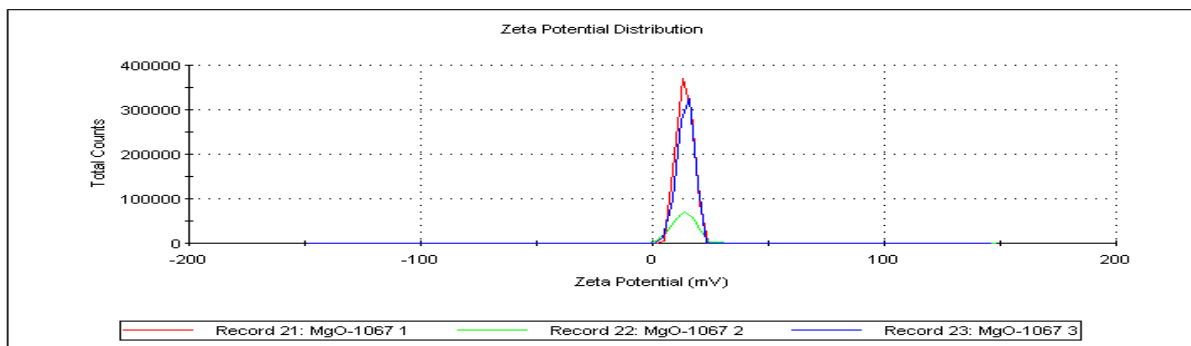


Sample Name: MgO-1067 3
SOP Name: MgO1067.sop
File Name: testing.dts
Record Number: 23
Date and Time: Tuesday, October 19, 2010 3:36:05 PM
Dispersant Name: Water
Dispersant RI: 1.330
Viscosity (cP): 0.8872
Dispersant Dielectric Constant: 78.6

Temperature (°C): 24.9
Count Rate (kcps): 142.6
Cell Description: Clear disposable zeta cell
Zeta Runs: 12
Measurement Position (mm): 2.00
Attenuator: 7

	Mean (mV)	Area (%)	Width (mV)
Zeta Potential (mV): 14.2	Peak 1: 14.2	100.0	3.51
Zeta Deviation (mV): 3.51	Peak 2: 0.00	0.0	0.00
Conductivity (mS/cm): 0.151	Peak 3: 0.00	0.0	0.00

Result quality: Good

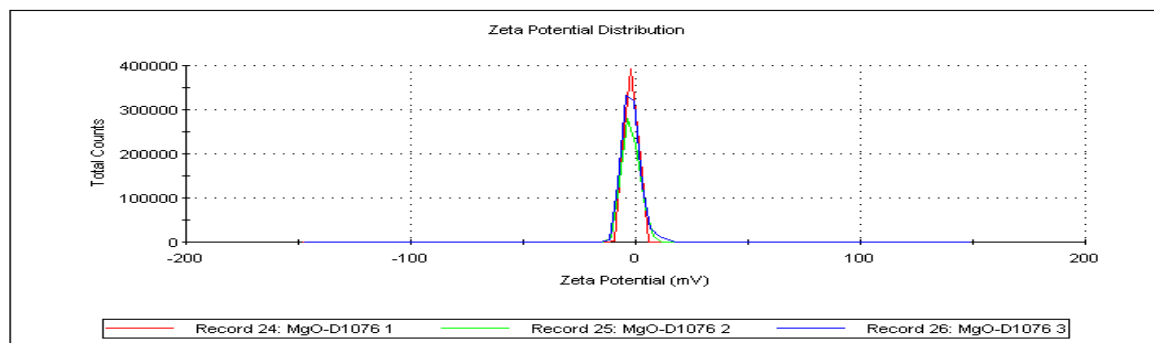


Sample Name: MgO-D1076 3
SOP Name: MgO-D1076.sop
File Name: testing.dts
Record Number: 26
Date and Time: Tuesday, October 19, 2010 3:44:30 PM
Dispersant Name: Water
Dispersant RI: 1.330
Viscosity (cP): 0.8881
Dispersant Dielectric Constant: 78.5

Temperature (°C): 25.0
Count Rate (kcps): 71.4
Cell Description: Clear disposable zeta cell
Zeta Runs: 12
Measurement Position (mm): 2.00
Attenuator: 7

	Mean (mV)	Area (%)	Width (mV)
Zeta Potential (mV): -2.08	Peak 1: -2.08	100.0	4.17
Zeta Deviation (mV): 4.17	Peak 2: 0.00	0.0	0.00
Conductivity (mS/cm): 0.249	Peak 3: 0.00	0.0	0.00

Result quality: Good

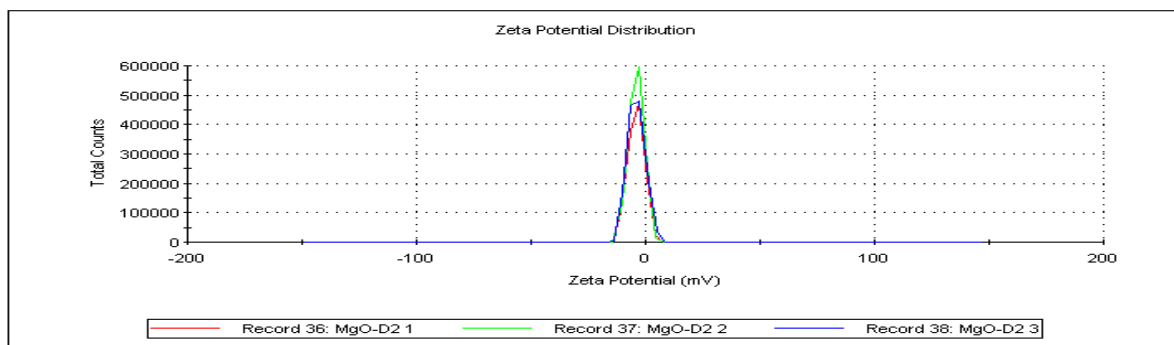


Sample Name: MgO-D2 3
SOP Name: MgO-D2.sop
File Name: testing.dts
Record Number: 38
Date and Time: Tuesday, October 19, 2010 4:15:39 PM
Dispersant Name: Water
Dispersant RI: 1.330
Viscosity (cP): 0.8878
Dispersant Dielectric Constant: 78.6

Temperature (°C): 25.0
Count Rate (kcps): 265.6
Cell Description: Clear disposable zeta cell
Zeta Runs: 12
Measurement Position (mm): 2.00
Attenuator: 6

	Mean (mV)	Area (%)	Width (mV)
Zeta Potential (mV): -4.03	Peak 1: -4.03	100.0	3.65
Zeta Deviation (mV): 3.65	Peak 2: 0.00	0.0	0.00
Conductivity (mS/cm): 0.266	Peak 3: 0.00	0.0	0.00

Result quality: Good

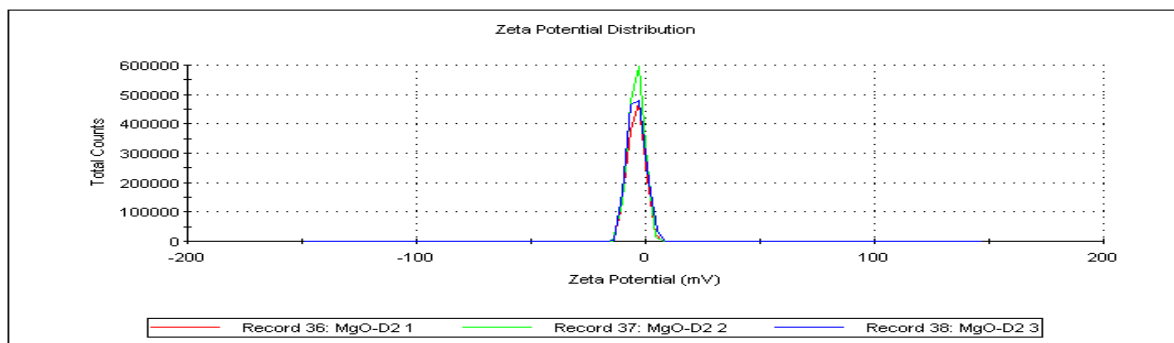


Sample Name: MgO-D2 3
SOP Name: MgO-D2.sop
File Name: testing.dts
Record Number: 38
Date and Time: Tuesday, October 19, 2010 4:15:39 PM
Dispersant Name: Water
Dispersant RI: 1.330
Viscosity (cP): 0.8878
Dispersant Dielectric Constant: 78.6

Temperature (°C): 25.0
Count Rate (kcps): 265.6
Cell Description: Clear disposable zeta cell
Zeta Runs: 12
Measurement Position (mm): 2.00
Attenuator: 6

	Mean (mV)	Area (%)	Width (mV)
Zeta Potential (mV): -4.03	Peak 1: -4.03	100.0	3.65
Zeta Deviation (mV): 3.65	Peak 2: 0.00	0.0	0.00
Conductivity (mS/cm): 0.266	Peak 3: 0.00	0.0	0.00

Result quality: Good

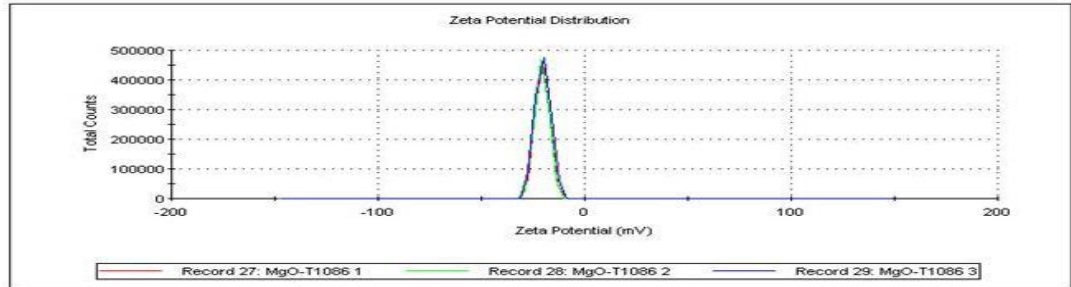


Sample Name: CuO 1086 3
SOP Name: CuO 1086.sop
File Name: testing.dts
Record Number: 29
Date and Time: Tuesday, October 19, 2010 3:50:54 PM
Dispersant Name: Water
Dispersant RI: 1.330
Viscosity (cP): 0.8865
Dispersant Dielectric Constant: 78.6

Temperature (°C): 25.0
Count Rate (kcps): 64.6
Cell Description: Clear disposable zeta cell
Zeta Runs: 12
Measurement Position (mm): 2.00
Attenuator: 6

	Mean (mV)	Area (%)	Width (mV)
Zeta Potential (mV): -20.3	Peak 1: -20.3	100.0	3.68
Zeta Deviation (mV): 3.68	Peak 2: 0.00	0.0	0.00
Conductivity (mS/cm): 0.287	Peak 3: 0.00	0.0	0.00

Result quality: Good

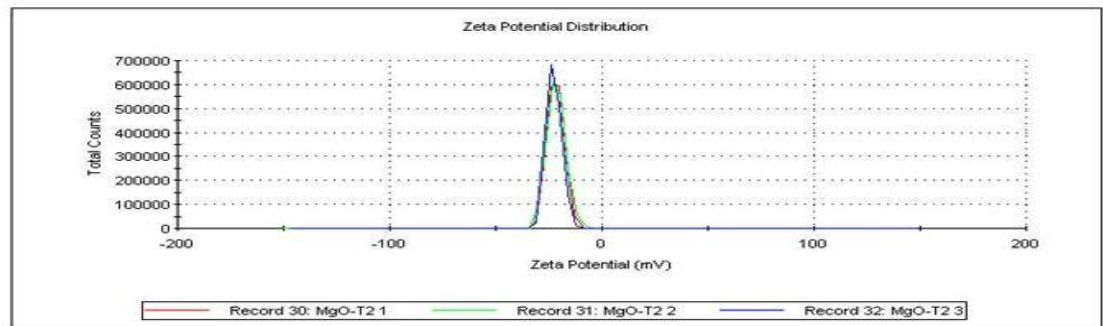


Sample Name: CuO.T23
SOP Name: CuO.T23
File Name: testing.dts
Record Number: 32
Date and Time: Tuesday, October 19, 2010 3:57:07 PM
Dispersant Name: Water
Dispersant RI: 1.330
Viscosity (cP): 0.8864
Dispersant Dielectric Constant: 78.5

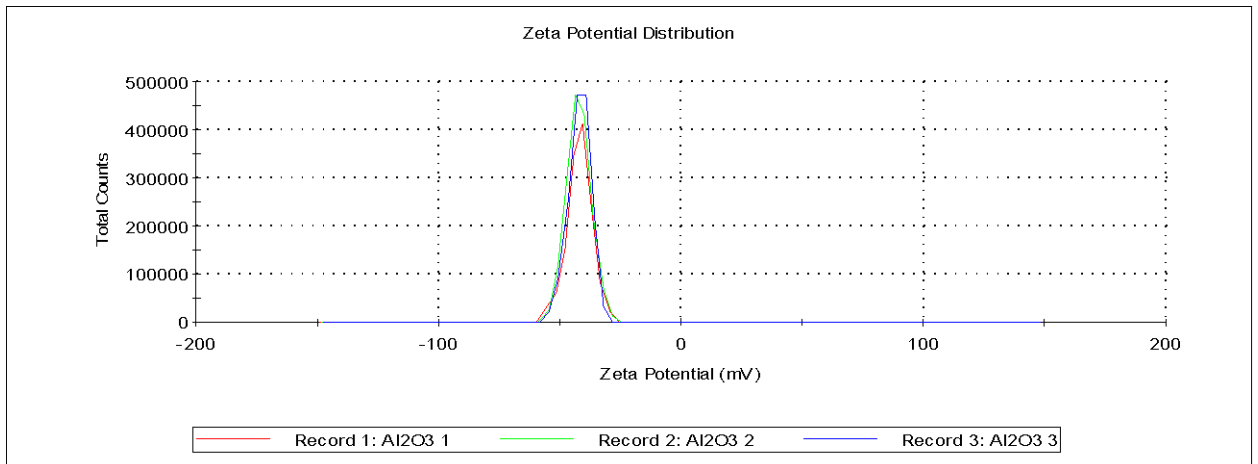
Temperature (°C): 25.0
Count Rate (kcps): 664.1
Cell Description: Clear disposable zeta cell
Zeta Runs: 12
Measurement Position (mm): 2.00
Attenuator: 6

	Mean (mV)	Area (%)	Width (mV)
Zeta Potential (mV): -22.7	Peak 1: -22.7	100.0	3.49
Zeta Deviation (mV): 3.49	Peak 2: 0.00	0.0	0.00
Conductivity (mS/cm): 0.333	Peak 3: 0.00	0.0	0.00

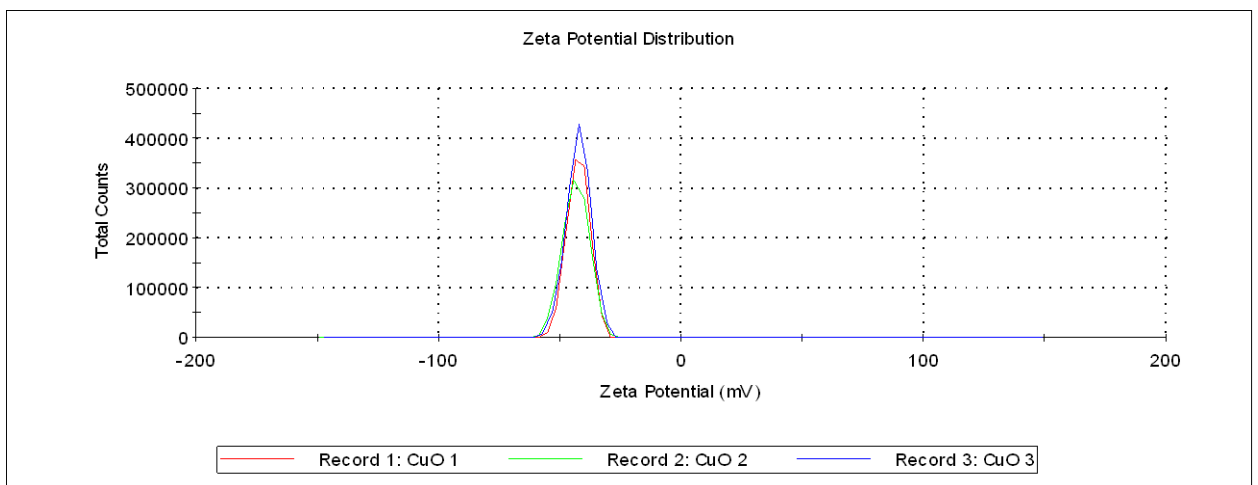
Result quality: Good



Record	Type	Sample Name	Measurement Date and Time	T °C	ZP mV	Mob μmcm/Vs	Cond mS/cm
1	Zeta	Al2O3 1	Saturday, November 14, 2009 11:02:19 AM	25.1	-41.9	-3.282	0.0396
2	Zeta	Al2O3 2	Saturday, November 14, 2009 11:05:11 AM	25.1	-42.2	-3.303	0.0401
3	Zeta	Al2O3 3	Saturday, November 14, 2009 11:06:50 AM	25	-41.7	-3.267	0.042
Mean 1-3				25.1	-41.9	-3.284	0.0406
Std Dev				0.1	0.252	0.01808	0.00127
RSD %				0.23	0.6	0.551	3.12
Minimum				25	-42.2	-3.303	0.0396
Maximum				25.1	-41.7	-3.267	0.042



Record	Type	Sample Name	Measurement Date and Time	T °C	ZP mV	Mob μmcm/Vs	Cond mS/cm
1	Zeta	CuO 1	Saturday, November 14, 2009 12:06:53 PM	25	-42.2	-3.311	0.025
2	Zeta	CuO 2	Saturday, November 14, 2009 12:09:46 PM	25.1	-43.3	-3.399	0.0309
3	Zeta	CuO 3	Saturday, November 14, 2009 12:11:25 PM	25	-42.3	-3.316	0.0279
Mean 1-3				25	-42.6	-3.342	0.0279
Std Dev				0.1	0.608	0.04943	0.00295
RSD %				0.231	1.43	1.48	10.6
Minimum				25	-43.3	-3.399	0.025
Maximum				25.1	-42.2	-3.311	0.0309

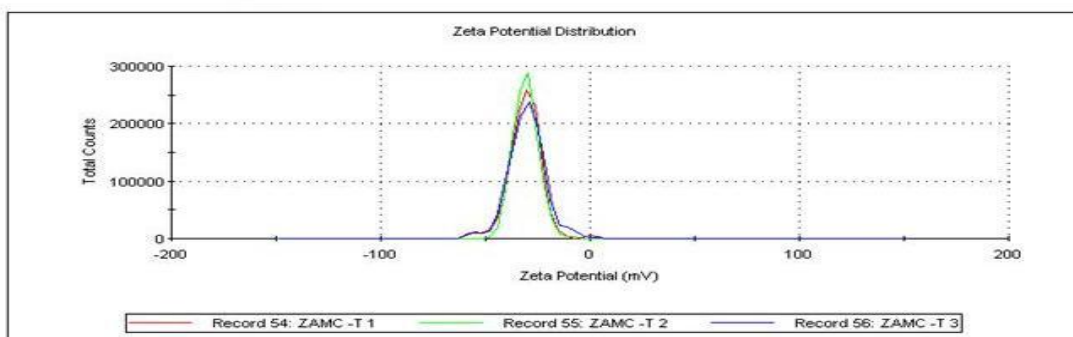


Sample Name: ZrO₂
SOP Name: ZrO₂. T.21
File Name: testing.dts
Record Number: 56
Date and Time: Tuesday, October 19, 2010 5:06:33 PM
Dispersant Name: Water
Dispersant RI: 1.330
Viscosity (cP): 0.8864
Dispersant Dielectric Constant: 78.5

Temperature (°C): 25.1
Count Rate (kcps): 151.0
Cell Description: Clear disposable zeta cell
Zeta Runs: 12
Measurement Position (mm): 2.00
Attenuator: 7

	Mean (mV)	Area (%)	Width (mV)
Zeta Potential (mV): -30.2	Peak 1: -29.8	97.7	8.32
Zeta Deviation (mV): 8.89	Peak 2: -55.1	2.3	2.95
Conductivity (mS/cm): 0.268	Peak 3: -32.1	0.0	0.00

Result quality : Good

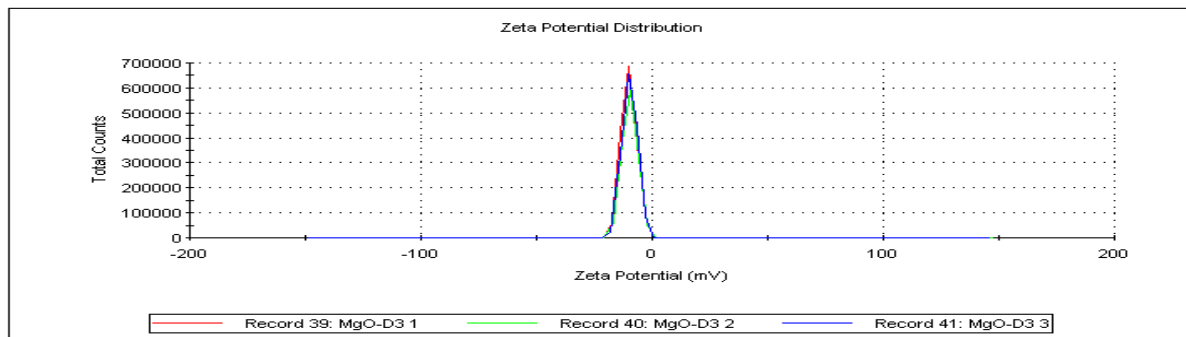


Sample Name: MgO-D3 3
SOP Name: MgO-D3.sop
File Name: testing.dts
Record Number: 41
Date and Time: Tuesday, October 19, 2010 4:23:00 PM
Dispersant Name: Water
Dispersant RI: 1.330
Viscosity (cP): 0.8878
Dispersant Dielectric Constant: 78.6

Temperature (°C): 24.9
Count Rate (kcps): 251.5
Cell Description: Clear disposable zeta cell
Zeta Runs: 12
Measurement Position (mm): 2.00
Attenuator: 7

	Mean (mV)	Area (%)	Width (mV)
Zeta Potential (mV): -9.79	Peak 1: -9.79	100.0	3.27
Zeta Deviation (mV): 3.27	Peak 2: 0.00	0.0	0.00
Conductivity (mS/cm): 0.351	Peak 3: 0.00	0.0	0.00

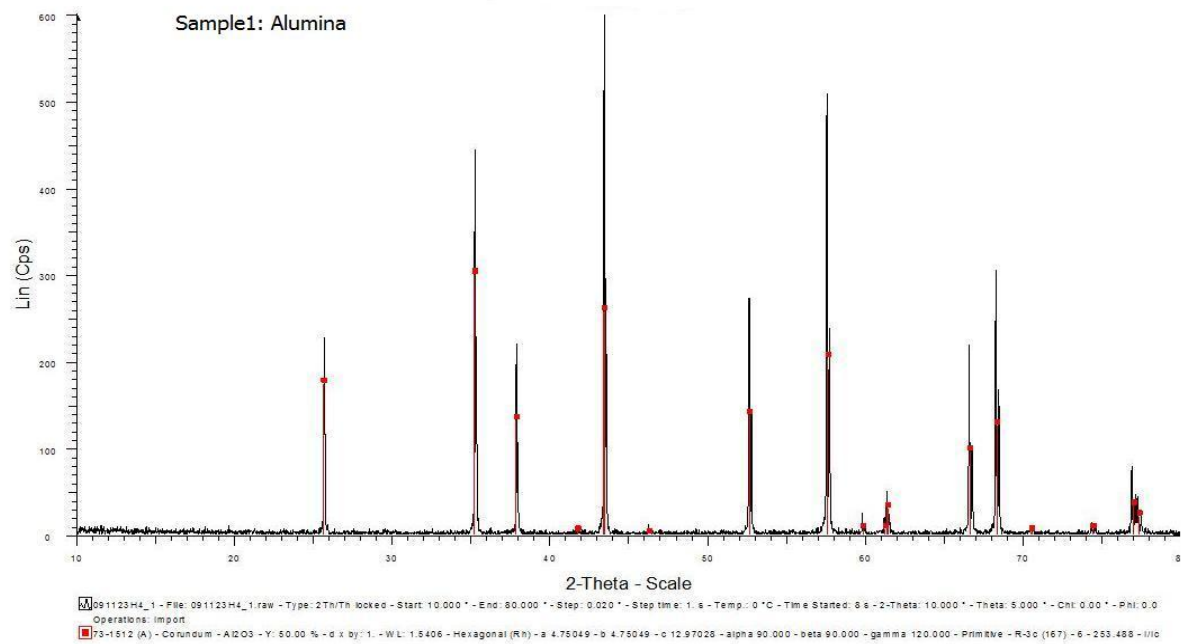
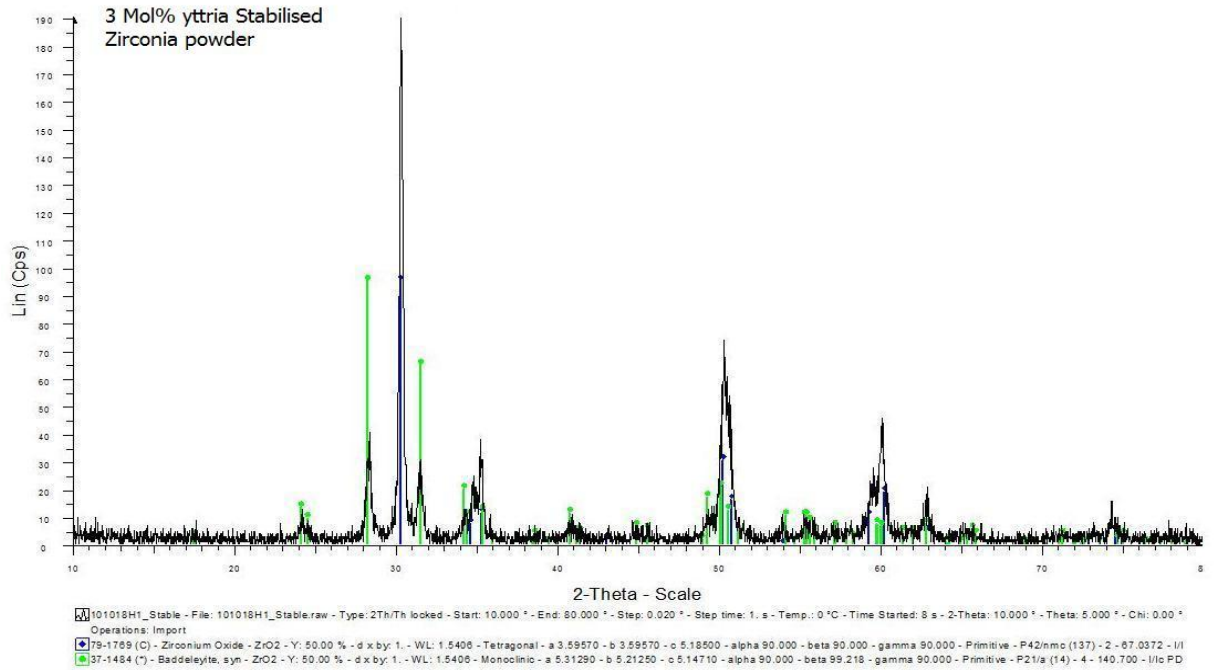
Result quality : Good

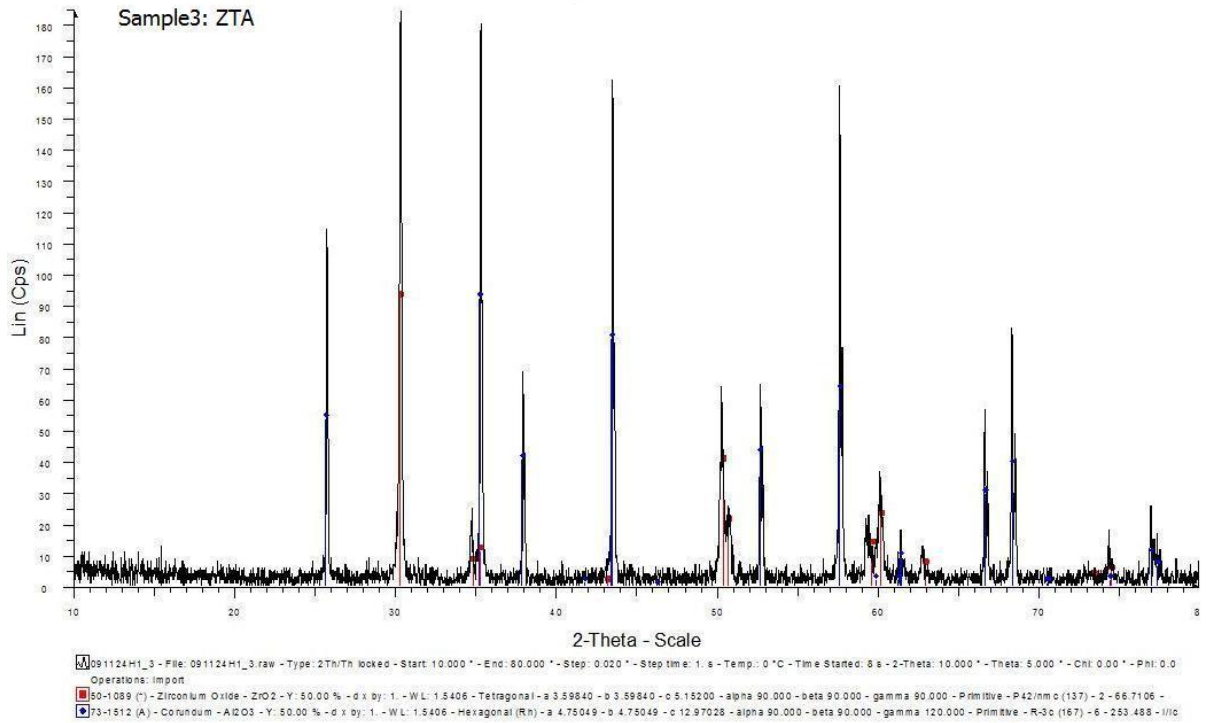
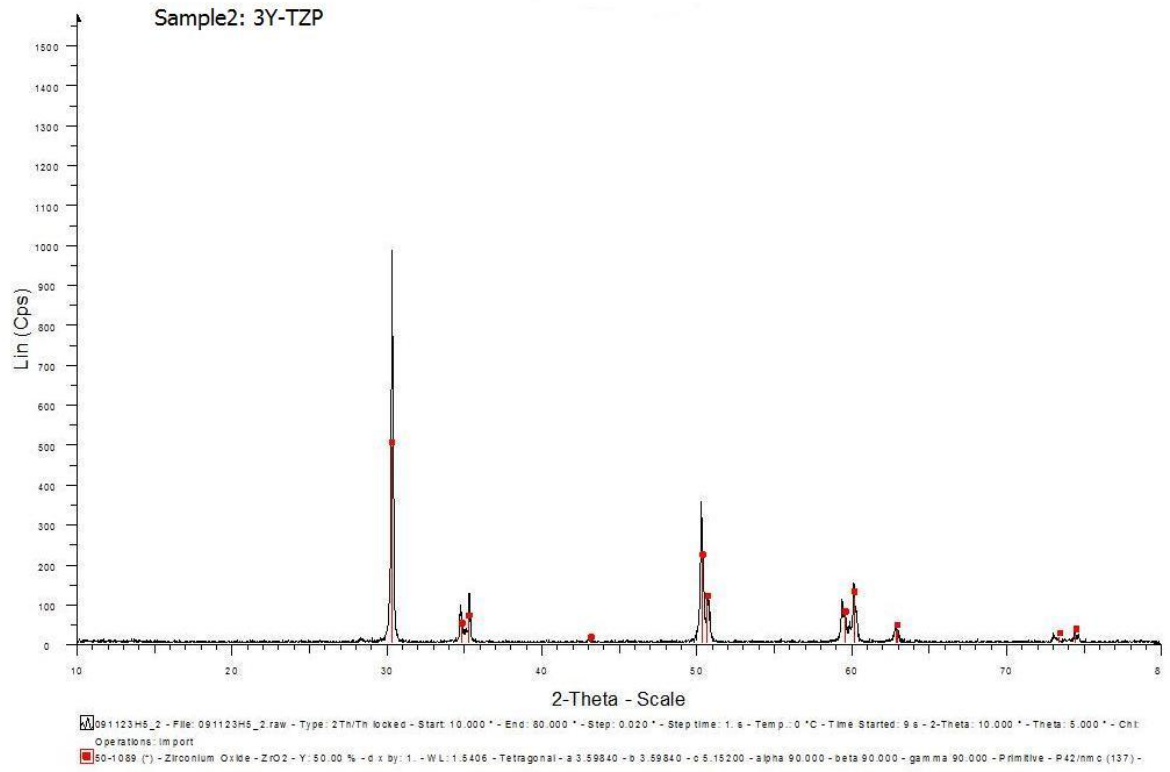


APPENDIX B: X-RAY DIFFRACTION

The pattern of X-Ray Diffraction for :

- 3 mol% yttria stabilized zirconia
- Alumina
- 3Y-TZP
- ZTA





APPENDIX C: SEM IMAGE OF VICKERS INDENTATION

